공학박사학위논문

Assembly of charged nanoparticles on a non-conducting substrate

비전도성 기판에서의 하전된 나노 입자의 조립

2016 년 2 월

서울대학교 대학원

기계항공공학부

강 승 현

비전도성 기판에서의 하전된 나노 입자의 조립

Assembly of charged nanoparticles on a non-conducting substrate

지도교수 최 만 수

이 논문을 공학박사 학위논문으로 제출함

2015 년 11 월

서울대학교 대학원

기계항공공학부

강 승 현

강승현의 공학박사 학위논문을 인준함

2015 년 12 월

위 원 장 : 이 준 식 (인)

부위원장 : 최 만 수 (인)

위 원 : 전 누 리 (인)

위 원 : 고 승 환 (인)

위 원 : 김 형 천 (인)

Assembly of charged nanoparticles on a non-conducting substrate

Seunghyon Kang
School of Mechanical and Aerospace Engineering
Seoul National University

Abstract

Assembly of nanoparticles has grabbed attention as an emerging microfabrication technique for its ability to directly manipulate and structure nanoscale building blocks that have unique size-dependent properties. Ion-assisted aerosol lithography is a versatile and scalable aerosol-based nanoparticle assembly technique. In spite of much development of Ion-assisted aerosol lithography, understanding of it on a non-conducting substrate has not been sufficiently investigated. In this study, we recognized the necessity of understanding about ion-assisted aerosol lithography on a non-conducting substrate for the wide use of this method. Hence, we have investigated the research about ion-assisted aerosol lithography on a non-conducting substrate.

First of all, the characteristics of ion-assisted aerosol lithography on a non-conducting substrate were investigated. Nanoparticle structure growth process on a non-conducting substrate was found to be self-terminate and subsequently, the structures repel incoming nanoparticles and scatter them away. Electric field calculations supported the experimental findings and confirmed that the electric field distortion which was caused by charge accumulation within the structures prevents deposition of additional nanoparticles on them.

In order to control accumulated charges on nanoparticle structures, we designed ion trap to manipulate the ion inflow. Through optimization of ion inflow, we have obtained the continuous growth of three-dimensional nanoparticle structures. The effect of charge accumulation on nanoparticle structures and resist surface was elucidated by electric field simulation.

Based on the understanding of ion-assisted aerosol lithography on a non-conducting substrate, we developed electrified mask method for large area on a non-conducting substrate. Multi-spark discharger and large area polymer electrified mask were used for large area assembly of charged nanoparticles. For the application of electrified mask to a non-conducting substrate, all the ions were eliminated by ion trap because electrified mask does not require ions for generation of electrostatic lenses. Applied electric potential on the electrified mask was calculated by electrified simulation. Consequently, we successfully demonstrated that the electrified mask method is applicable to a non-conducting substrate as well as to a conducting substrate. Moreover, precise control of focusing ratio was also achieved on a non-conducting substrate.

Keywords: Nanoparticle assembly, Non-conducting substrate, ion-assisted aerosol lithography, ion trap, electrified mask

Student Number: 2009-20649

Contents

List of Table

Nomenclature

A_H	Hamaker constant	
C_c	Cunningham correction factor	
d_p	particle diameter	[nm]
e	charge of an electron	[1.602×10^{-19} C]
$\boldsymbol{E}$	electric field strength	[V/m]
E_{um}	electric field strength under the mask	[V/m]
E_{om}	electric field strength over the mask	[V/m]
f	friction coefficient	
$\boldsymbol{F}_B$	Brownian force	[N]
$\boldsymbol{F}_C$	Coulomb force	[N]
$\boldsymbol{F}_D$	drag force	[N]
$\boldsymbol{F}_E$	electric force	[N]
$\boldsymbol{F}_{vdW}$	van der Waals force	[N]
k_B	Boltzmann constant	[1.381×10^{-23} J/K]
m_p	mass of particle	[kg]
n	number of elementary charge	
q	magnitude of charges	[C]
Re	Reynolds number	
r_e	ratio of	
T	temperature	[K]

t	time	[sec.]
Δt	time step	[sec.]
V_B	breakdown voltage	[V]
$V_{electrode}$	electric potential at the electrode	[V]
v_g	flow velocity	[m/s]
V_{mask}	electric potential at the mask	[V]
$V_{substrate}$	electric potential at the substrate	[V]
V_{TE}	terminal velocity	[m/s]
v_p	particle velocity	[m/s]
Z	electrical mobility	[m^2/V·s]

Greek Symbols

γ	Townsend coefficient
λ	mean free path of the gas
μ	viscosity of the gas
ξ	zero-mean, unit-variance Gaussian random number
ρ	charge density

List of Figures

Chapter 1.

Introduction

1.1. Background of Research

Assembly of nanoparticles has grabbed the much attention around the world as emerging microfabrication technique for its capability to directly manipulate and structure nanoscale building blocks. Numerous methods of nanoparticle assembly have been developed, taking advantage of physical forces such as electrostatic forces (Kalsin et al. 2006; Kim et al. 2006; Jiang et al. 2009), magnetic forces (Wolf and Birringer 2005; Demirors et al. 2013), capillary forces (Lin et al. 2003; Vyawahare et al. 2006; Kraus et al. 2007; Su et al. 2014), and selective molecular bonding (Nykypanchuk et al. 2008). The unique properties of nanoparticle structure have been utilized in various applications such as photonics (Ergin et al. 2010; von Freymann et al. 2010; Zhang et al. 2011), gas sensing (Ponzoni et al. 2006; Kim et al. 2011), and Li batteries (Park et al. 2010; Guo et al. 2011).

Ion-assisted aerosol lithography is a versatile and scalable aerosol-based nanoparticle assembly technique which enables fabrication of three-dimensional nanoparticle structures (Kim et al. 2006, Lee et al. 2011).

Charged nanoparticles and ions are sprayed on the Si substrate with a pre-patterned photoresist layer, and they are attracted to the substrate by the electrical attractions. The ions are arrived on the substrate first by the electrical mobility difference, and remained ions on the surface of the photoresist pattern distorts the electric field around the openings. The charged nanoparticles that arrive later follow electric field streamlines to be deposited at the center of each photoresist pattern opening. Eventually, the nanoparticles pile up to form three-dimensional structures with re-entrant and/or slanted features.

Using the ion-induced focusing mask, high-resolution array of nanoparticles can be obtained by sequential deposition of nanoparticles (You et al. 2010). Since the

electrostatic lenses are generated on the floated mask which is separated from the substrate, the electrostatic lenses can be translated relative to the substrate. Therefore, high density of nanoparticle assembly array can be obtained through sequential operation with translation of the mask, and focusing mask can be used repeatedly since the nanoparticles are selectively deposited onto the substrate, not on the mask, which eliminates the need to prepare a new mask for each operation.

Electrified mask is advanced form of ion-induced focusing mask (Choi et al. 2015). In this method, electrostatic lenses are generated by applying an electric potential to metal coated stencil mask. Therefore, not only electrified mask has advantages of ion induced focusing mask, but also it has one another great advantage which is precise control of electrostatic lenses by adjusting applied potential.

In our laboratory, aerosol-based nanoparticle assembly technique has been developed substantially since it was first reported. However, ion-assisted aerosol lithography has been limited to conducting substrates because the study about the ion-assisted aerosol lithography on a non-conducting substrate has not been sufficiently investigated. A restriction of substrate type is a critical shortcoming of nanoparticle assembly technique which has an object of various application. You et al. (2010) demonstrated ion-assisted aerosol lithography on a non-conducting substrate by employing a conducting liquid layer to conduct away the charges; however, it required a substrate with hydrophilic surfaces to form a continuous liquid layer, thereby complicating the substrate choice and/or preparation. Therefore, it is necessary to investigation of charged particle assembly method on a non-conducting substrate without any restrictions.

1.2. Objectives for Research

The objective of this research is widening the use of charged nanoparticle assembly method into a non-conducting substrate. In ion-induced focusing method, electrical properties of each components is very important, because this method utilize electric filed to control movement of nanoparticles. Therefore, this method has been limited to conducting substrate, or restrictively applied to a non-conducting substrate due to insufficient investigation of the study about the ion-induced focusing method on a non-conducting substrate. To make up this disadvantage of ion-induced focusing method, a restriction of substrate type should be overcome.

In order to achieve this objective, our research is progressed through dividing the topic into three parts; understanding principle of charged nanoparticle assembly on a non-conducting substrate via ion induced focusing method, fabrication of three-dimensional nanoparticle assembly on a non-conducting substrate via ion-assisted aerosol lithography, and large area charged nanoparticle assembly on a non-conducting substrate via the electrified mask. Detailed description of each part is demonstrated in next section.

1.3. Scope of Research

In order to expand applicability of ion-induced focusing method to a non-conducting substrate, our research is progressed through dividing the topic in three parts.

At first, we investigated principle of ion-induced focusing method on a non-conducting substrate in Chapter 2. We figured out a difference between the cases which ion-assisted aerosol lithography was performed on a conducting and a non-conducting substrate. Through the electric field simulation, principle of three-dimensional nanoparticle structure growth on a non-conducting substrate was explained, and we found out that ion accumulation on a nanoparticle structure is primary factor which caused terminating of three-dimensional nanoparticle structure growth on a non-conducting substrate.

In Chapter 3, we successively obtained three-dimensional nanoparticle structure on a non-conducting substrate without a terminating. An ion trap was designed and used to control ion accumulation. We showed that the ion trap could control ion inflow through selective capture of ions by electrical mobility difference between ions and nanoparticles. The different experimental results depend on the ion inflow were explained through electric field simulation results. Consequently, three-dimensional nanoparticle structure on a non-conducting substrate could be obtained by optimization of ion inflow.

Charged nanoparticle assembly method on a non-conducting substrate via electrified mask was studied and large area charged nanoparticle assembly system was designed for wide use of this method, in Chapter 4. A large area charged nanoparticle assembly system was comprised of multi-spark discharger system and large area polymer electrified mask. Because electrified mask was not required ions

for generation of electrostatic lenses, charged nanoparticle assembly on a non-conducting substrate via electrified mask could be obtained by complete elimination of ions. We showed that focusing ratio could be controlled by manipulating of applied potential even in the case of the non-conducting substrate. The characteristics of electrified mask method on a non-conducting substrate were elucidated through electric field simulation.

Chapter 2.

Characteristics of ion-assisted aerosol lithography on a non-conducting substrate

2.1. Introduction

Ion-assisted aerosol lithography is aerosol-based nanoparticle assembly technique which can produce high resolution and three-dimensional nanoparticle assembly array (Kim et al. 2006; Lee et al. 2009; Lee et al. 2011). Charged nanoparticles can be guided to desired position through an electrostatic lens which is generated from the accumulated ions on a resist surface. Thus, ion-assisted aerosol lithography method utilizes electric field distortion to control movement of charged nanoparticle. Hence, the electrical properties of each component are very important for ion-assisted aerosol lithography. Especially, a conductivity of a substrate is a key parameter of this method, because it directly has effect on the ion accumulation and electric field formation. For this reason, the ion-assisted aerosol lithography has been limited to a conducting substrate, or restrictively applicable to a non-conducting substrate with complicating selection of substrate and/or preparation (You et al. 2010). In order to enhance practical use of this method, a limitation of substrate type should be overcome. To achieve this objective, an in-depth study of ion-assisted aerosol lithography on a non-conducting substrate is required first.

In this work, we attempted to assembly of charged nanoparticles on a non-conducting substrate by using previous ion-assisted aerosol lithography method. It was observed that growth of nanoparticle structures was terminated with scattered nanoparticles on a resist surface. Based on the understanding of an electric field formation on a non-conducting substrate and applied forces on nanoparticles, we could have elucidated that this termination was originated from charge accumulation on the nanoparticle structures. It is fully backed up by electric field simulation.

2.2. Experimental concept

2.2.1. Ion-assisted aerosol lithography

Ion-assisted aerosol lithography is an aerosol based nanoparticle assembly technique (Kim et al. 2006). Figure 2.1 shows schematic for ion-assisted aerosol lithography. The charged nanoparticles and ions are injected into a deposition chamber and they are dragged to a substrate by electric attraction. Due to electrical mobility difference, ions are arrived first at the substrate, then they are deposited on surface and inside of pre-patterned resist pattern. The charges on exposed surface of a substrate are escaped through the electrode, thus only the charges which are accumulated on the surface of resist pattern is remained. Electrostatic lenses are generated by accumulated charges on the resist surface. The charged nanoparticles that arrived later guided into center of the opening in the resist pattern through the electrostatic lenses. The feature sizes of the nanoparticle patterns are significantly smaller than those of the original resist pattern. Therefore, high resolution patterns can be obtained through the ion-assisted aerosol lithography (Figure 2.2).

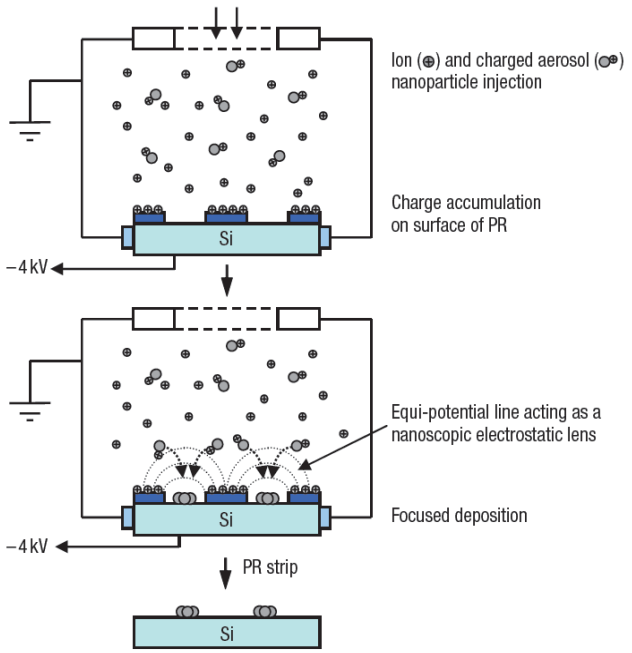

Figure 2.1. Schematic for ion-assisted aerosol lithography (Kim et al. 2006)

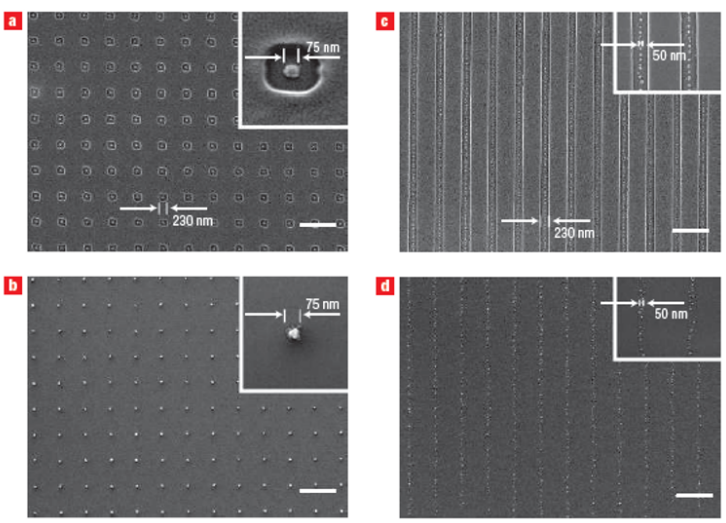

Figure 2.2. Particle patterning results via ion-assisted aerosol lithography (Kim et al. 2006)

Formation of three-dimensional nanoparticle assembly can be obtained by continuous deposition of nanoparticles (Lee et al. 2011). Figure 2.3a shows numerical calculation results of particle trajectories during the process of three-dimensional nanoparticle structure growth. The electric potential of deposited particles becomes equal with electric potential of the electrode. Thus, the electric field near the deposited particles is enhanced. Consequently, the enhanced electric field near the surface of the deposited particles play a role in constructing three-dimensional nanoparticle structures, and this effect defined as the antenna effect (Lee et al. 2011). Figure 2.3b shows time-dependent growth of three-dimensional nanoparticle structure array. A variety three-dimensional nanoparticle structure could be obtained via ion-assisted aerosol lithography.

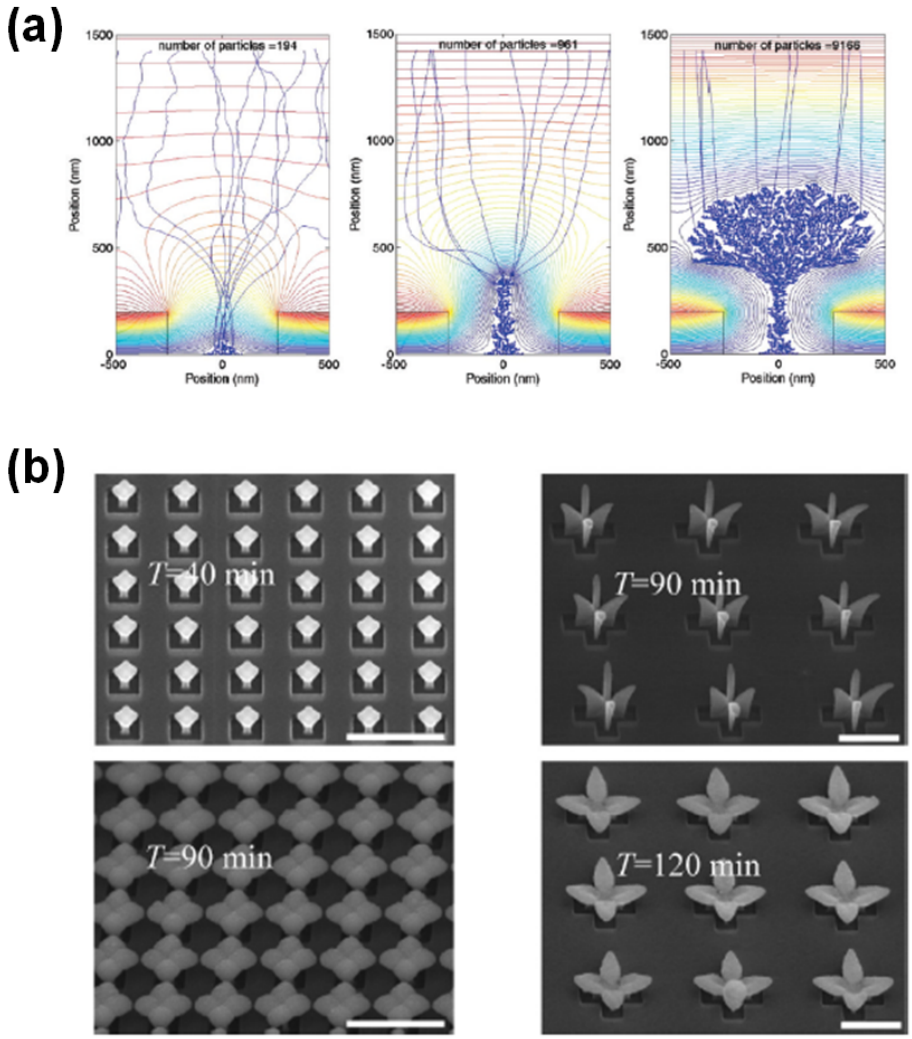

Figure 2.3. (a) Numerical calculation results of particle trajectories during the process of three-dimensional nanoparticle structure growth. (b) Time-dependent growth of three-dimensional nanoparticle structure array (Lee et al. 2011).

2.2.2. Governing equation of charged nanoparticles during the process of ion-assisted aerosol lithography

Ion-assisted aerosol lithography utilize an electric force to control movement of charged nanoparticles. Incoming charged nanoparticles can be manipulated by electrostatic lenses produced from accumulated ions. Hence, an electric force and a drag force apply to charged nanoparticles during ion-assisted aerosol lithography. Therefore, the governing equation for particle motion is

$$m_p \frac{d\overrightarrow{\boldsymbol{v}_p}}{dt} = \overrightarrow{\boldsymbol{F}_D} + \overrightarrow{\boldsymbol{F}_E} + \overrightarrow{\boldsymbol{F}_B} + \overrightarrow{\boldsymbol{F}_{vdW}} \tag{2.1}$$

where m_p is mass of the particle, $\overrightarrow{v_p}$ is velocity of the particle, $\overrightarrow{\boldsymbol{F}_D}$ is the drag force, $\overrightarrow{\boldsymbol{F}_E}$ is the electrostatic force, $\overrightarrow{\boldsymbol{F}_B}$ is the Brownian force, and $\overrightarrow{\boldsymbol{F}_{vdW}}$ is van der Waal's force.

The drag force exerted on spherical particles with very small Reynolds number ($\mathrm{Re} = \rho v_p d_p/\mu$) can be explained using Stokes' law (Hinds, 1999).

$$\boldsymbol{F}_D = 3\pi\mu d_p(v_g - v_p) \quad \text{for } \mathrm{Re} < 1 \tag{2.2}$$

where μ is viscosity of the gas, v_g is flow velocity, v_p is particle velocity, and d_p is diameter of the particle. When the resisting force is applied to a particle, as described in Eq. 2.2, the particle motion is said to be in the Stoke region. There is important assumption in Stokes' law. The relative velocity of the gas right at the surface of the sphere should be zero. However, when the particle size approaches the mean free path of the gas, this assumption is inapplicable. Therefore, when the

particle size is smaller than 0.1 μm in diameter, the drag force equation should be used *Cunningham correction factor* (C_c) to account for effect of slip. Thus,

$$\boldsymbol{F}_D = f(v_g - v_p) \tag{2.3}$$

$$f = \frac{3\pi\mu d_p}{C_c} \tag{2.4}$$

where

$$C_c = 1 + \frac{\lambda}{d_p}\left[2.34 + 1.05exp\left(-0.39\frac{d_p}{\lambda}\right)\right] \tag{2.5}$$

f is friction coefficient, and λ is the mean free path of the gas.

The electrostatic force of charged particles with n elementary units of charge in an electric field is

$$\boldsymbol{F}_E = qE = neE \tag{2.6}$$

where q is the charge on the particle, E is electric field strength, and e is the charge on an electron (1.6×10^{-19} C).

The Brownian force is

$$\boldsymbol{F}_B = \sqrt{\frac{2k_BTf}{\Delta t}}\xi \tag{2.7}$$

where k_B is Boltzmann constant, T is temperature, and ξ is a zero-mean, unit-variance Gaussian random number (Li & Ahmadi, 1992).

The van der Waal's force ($\boldsymbol{F}_{vdW}$) is

$$\boldsymbol{F}_{vdW} = \frac{A_{H_{pgp}} d_p^3}{12\left(D_{C-S} - \frac{d_p}{2}\right)^2 \left(D_{C-S} + \frac{d_p}{2}\right)^2}\boldsymbol{n} + \frac{A_{H_{pgp}} d_p^6}{6\left(D_{C-C} - d_p\right)^2 D_{C-C}^3 \left(D_{C-C} + d_p\right)^2}\boldsymbol{r} \qquad (2.8)$$

where A_H is the Hamaker constant (Visser, 1972).

2.3. Experimental method

2.3.1. Fabrication of a non-conducting substrate

To investigate the characteristics of ion-assisted aerosol lithography on a non-conducting substrate, a Si substrate with 500 nm of thermally grown SiO_2 layer was used (Figure 2.4). A 100 nm thick e-beam resist pattern was fabricated on the SiO_2 layer (Figure 2.4b), while it was fabricated on the Si conducting substrate in the case of previous ion-assisted aerosol lithography method on a conducting substrate (Figure 2.4a). The e-beam resist (ER) pattern which have 200 nm opening and 400 nm spacing was fabricated by e-beam lithography.

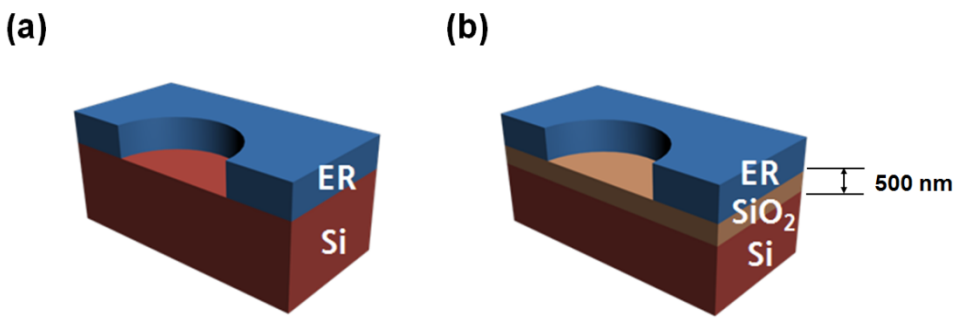

Figure 2.4. Structures of (a) a conducting substrate and (b) a non-conducting substrate

2.3.2. Particle generation and assembly

Fig.2.5a shows the experimental set-up for nanoparticle generation and assembly via ion-assisted aerosol lithography on a non-conducting substrate. The pin-plate spark discharger was used to generate charged Ag nanoparticles (Han et al. 2012). The pin and plate electrode were fabricated using 99.9% purity silver rod and foil (Alfa Aesar, Ward Hill, MA, USA). Charged Ag nanoparticles having a geometric mean diameter of 4.3 nm (Figure 2.5b) were generated at following system parameters: resistivity, 10 MΩ; capacity, 2 nF; Applied voltage to the spark discharge control circuit (HV1), 4.5 kV; nitrogen flow, 1 lpm. Nitrogen ions were generated by the corona discharger with 3.5 kV (HV2) and 1 lpm.

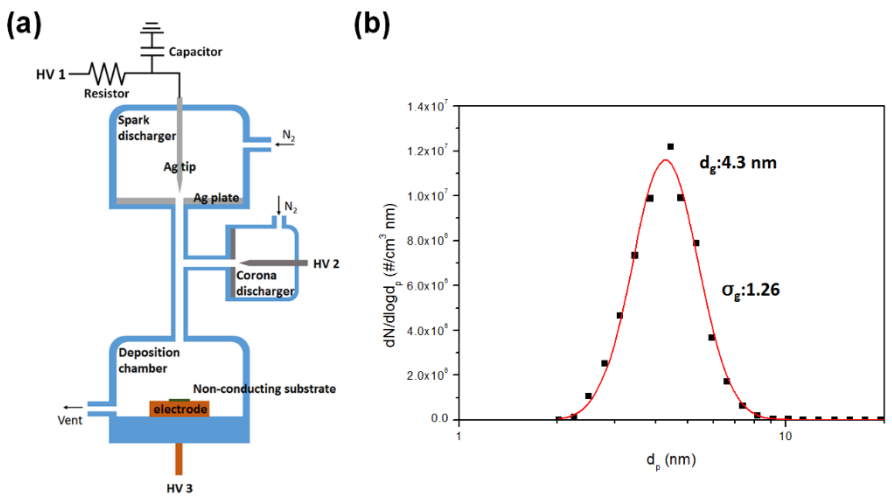

Figure 2.5. (a) Experimental set-up for ion-assisted aerosol lithography on a non-conducting substrate. (b) Particle distribution of Ag nanoparticles which was generated from pin-to-plate spark discharger

Particle size distribution was measured using the scanning mobility particle sizer (SMPS, Model 3080, TSI Inc., USA) system which was comprised of a neutralizer (Model 3077, TSI Inc., USA), a differential mobility analyzer (Model 3085, TSI Inc., USA), and a condensation particle counter (Model 3776, TSI Inc., USA).

The charged Ag nanoparticles and nitrogen ions were injected into a deposition chamber and they were dragged to substrate with electrode voltage at -2 kV (HV3). The ions arrived first at the substrate because the electric mobility of ions was much larger than that of the nanoparticles. Then, electrostatic lenses were generated by the ions which were accumulated on the pre-patterned resist surface (Kim et al., 2006). The charged nanoparticles that arrived later follow the electric field streamlines and guided toward the center of the opening in the resist pattern (Lee et al. 2009). Three-dimensional nanoparticle structures were obtained by a continuous deposition of the nanoparticles (Lee et al. 2011).

The results of nanoparticle assembly were observed using field-emission scanning electron microscopy (FE-SEM, Merlin Compact, Carl Zeiss, Oberkochen, Germany) at an acceleration voltage of 2 kV.

2.3.3. Electric field simulation

Electric field simulations were performed using electrostatic modules of COMSOL multiphysics 4.4 in order to understand the principle of three-dimensional nanoparticle structure growth on a non-conducting substrate. The simulation volume was defined as a cuboid (600 nm × 600 nm × 1600 nm) which encloses a sufficient volume around a single resist pattern opening. The electric field distribution within the deposition chamber was calculated and it was used to the electric potential boundary condition at the top surface of the simulation volume (Figure 2.6).

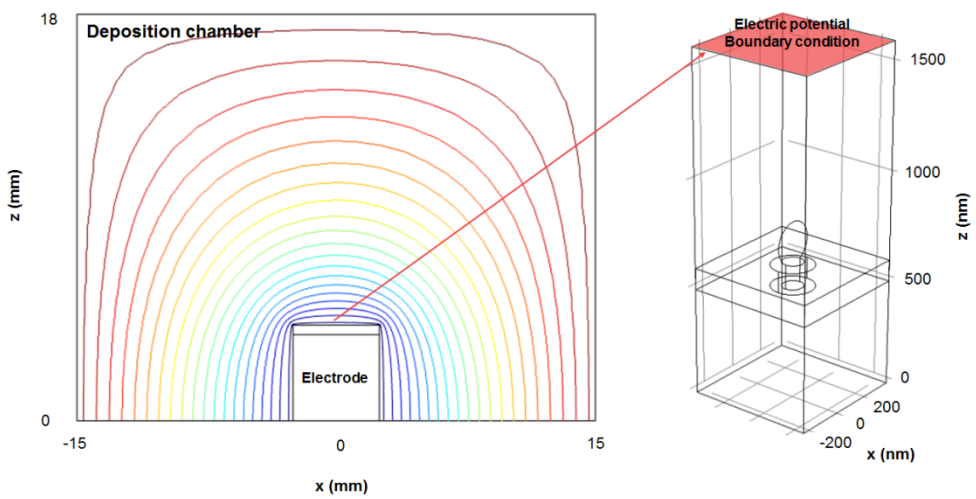

Figure 2.6. Set-up of electric field simulation volume. The electric potential boundary condition at the top surface of simulation volume was obtained from electric field distribution of the deposition chamber

The ions were assumed to be saturated on the resist surface when no additional ion deposition is allowed on the surface and the surface charge density needed to achieve this was calculated to be approximately 2.3×10^{-4} C/m^2 (Figure 2.7).

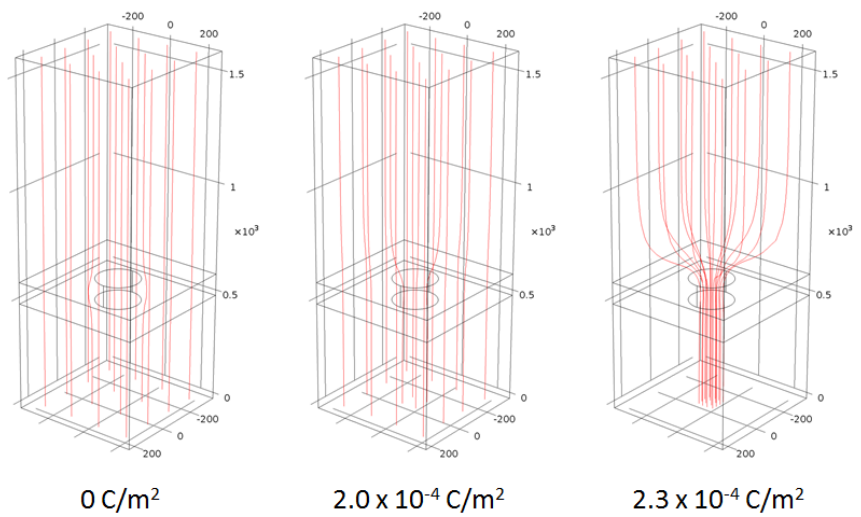

Figure 2.7. Calculation of surface charge density on top of the resist pattern and the exposed SiO_2 surface

2.4. Results and discussion

2.4.1. Electrostatic focusing of charged nanoparticles on a non-conducting substrate

Figure 2.8 shows the results of three-dimensional nanoparticle structure depends on the growth time. Up to 60 minutes, the nanoparticle structures were enlarged as the deposition time increased (Figure 2.8a-c). However, at 120 minutes, scattered nanoparticles on the resist surface were found far away from the nanoparticle structures (Figure 2.8d), which cannot be shown in the case of ion-assisted aerosol lithography on a conducting substrate (Lee et al. 2011). This unique phenomenon was originated from the non-conductivity of the substrate. These results imply that there is a certain point where the charged nanoparticles start to get repelled from the nanoparticle structures instead getting attracted, which eventually leads to termination of their growth between the growth times of 60 to 120 minutes.

When the nanoparticle structure was assembled on a conducting substrate via ion-assisted aerosol lithography, the charges in the nanoparticle structure could escape through the conducting substrate which was electrically connected to the electrode. Whereas, the electrical path was blocked by the non-conducting substrate. As a result, the charges were accumulated on the nanoparticle structures, and these accumulated charges caused the termination of their growth. Therefore, it suggests that the charges from nanoparticles and ions accumulate within the nanoparticle structures as the growth proceeds and eventually, the accumulated charge becomes large enough to repel the incoming nanoparticles. To validate this hypothesis, we performed electric field simulation and compared the results to the experiments.

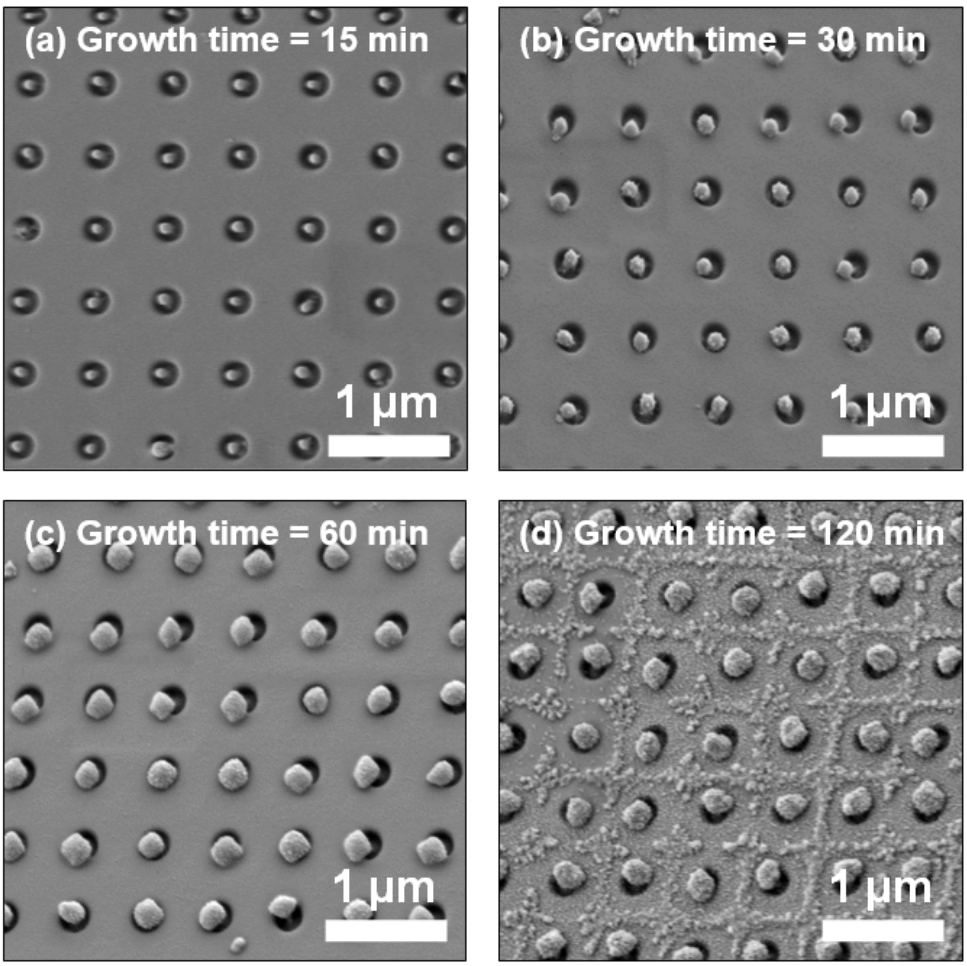

Figure 2.8. SEM images of procedure nanoparticle structure growth on a non-conducting substrate via ion-assisted aerosol lithography

2.4.2. Electric field distortion during assembly of charged nanoparticles on a non-conducting substrate

The electric field simulation results for ion-assisted aerosol lithography on a non-conducting substrate were shown at Figure 2.9. There are three stages in the nanoparticle structure growth. Initially, the charged nanoparticles and ions were injected to the deposition chamber. The ions get to the substrate first and then the rest of nanoparticles get to the substrate due to its difference in electrical mobility. The ions are deposited on the resist surface as well as the exposed SiO_2 surfaces inside the resist patterns. Even though all of the charges were not being removed, electrostatic lenses were well generated because of a spatial charge distribution arising from the height difference between the top of the resist pattern and the exposed SiO_2 surface (Figure 2.9a).

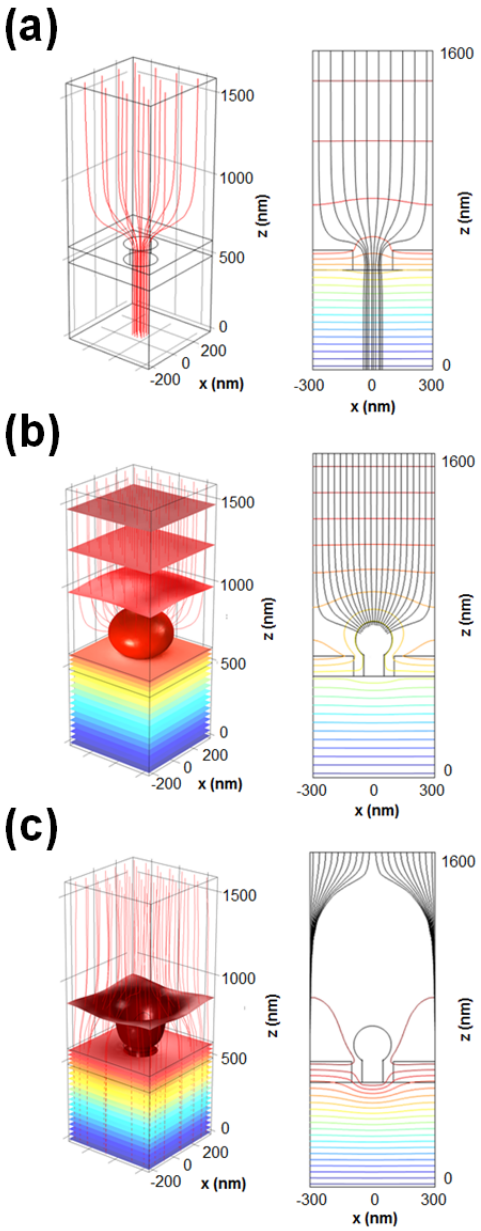

Figure 2.9. Electric field simulation results for ion-assisted aerosol lithography on a non-conducting substrate. The three stages of nanoparticle structure growth: (a) initial growth, (b) steady growth, and (c) growth termination

As the structure grows, structure-particle interactions start to play a significant role in addition to the electrostatic lens effect. Figure 2.10 shows different principle of structure-particle interaction for a conducting and a non-conducting substrate.

In the case of the conducting substrate, the metal nanostructure was electrically connected to the electrode through the conducting substrate (Figure 2.10a). Therefore, electric potential of the nanoparticle structure had same value with the applied voltage (HV3 of Figure 2.5a). This electric potential enabled to attract following charged nanoparticles with relatively strong force which was defined as the antenna effect (Lee et al. 2011). However, when nanoparticle structure was grown on non-conducting substrate, it could not connected to the electrode by the insulating layer (Figure 2.10b). Thus, the three-dimensional nanoparticle structure existed in the floating status in static electric field. When the metal (or conductor) was floated in static electric field, the free charges in the metal were moved by the external electric field. Hence, a conductor has charges only on its surface and there are no charges inside a conductor ($\rho = 0$). According to Gauss's law, electric field in the interior of a conductor must be zero ($E = 0$) because the total outward electric flux through any closed surface constructed inside the conductor must vanish. As a result, the surface and volume of a conductor are equipotential (Cheng 1989). By this equipotential surface, the following nanoparticles could be attracted to the nanostructure, but the force was relatively weak than that of the antenna effect (Figure 2.9b).

The attraction grows weaker as more charges are accumulated on the nanoparticle structure. Eventually, the structure's surface potential becomes large enough to deflect electric field stream lines away from them (Figure 2.9c) at which point the growth stops and the incoming nanoparticles are repelled and scattered on the resist surface. Thus, to induce continuous growth of the nanoparticle structure on a non-

conducting substrate, it is necessary to control charge accumulation in the nanoparticle structure.

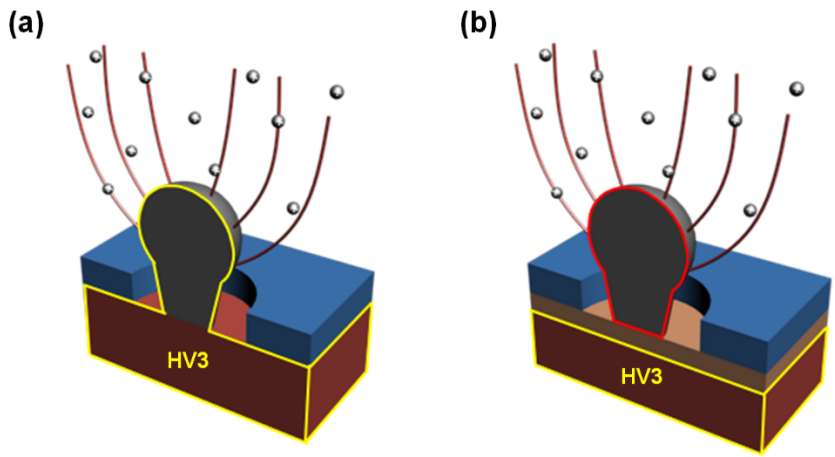

Figure 2.10. Principle of particle-structure interaction in the case of (a) conducting substrate and (b) non-conducting substrate

2.5. Conclusion

We investigated characteristics of ion-assisted aerosol lithography on a non-conducting substrate. When the charged nanoparticles were assembled on a non-conducting substrate via ion-assisted aerosol lithography, scattered nanoparticles on the resist surface were observed far away from the nanoparticle structure. We found out that there was a point where the charged nanoparticles started to get repelled from the nanoparticle structures instead of being attracted to them, terminating their growth. We supposed that accumulated charges in nanoparticle structures caused this termination of nanoparticle structure growth. Through the electric field simulation, we understood the principle of nanoparticle structure growth on a non-conducting substrate and verified that the charge accumulation in nanoparticle structure played a critical role in this termination of nanoparticle structure growth. As the nanoparticle structure growth proceeded, the electric potential on nanoparticle structures increased by accumulation of charges from nanoparticles and ions. Eventually, the electric potential on nanoparticle structures became large enough to repel incoming nanoparticles. Therefore, we can conclude that the control of charge accumulation in nanoparticle structures was necessary for the continuous growth of nanoparticle structure on a non-conducting substrate.

Chapter 3.

Assembly of three-dimensional nanoparticle structures on a non-conducting substrate via ion-assisted aerosol lithography

3.1. Introduction

Applicability of ion-assisted aerosol lithography has been limited to a conducting substrate, or restrictively applicable to a non-conducting substrate with complicating selection of substrate and/or preparation (You et al. 2010). In order to enhance practical use of this method, above restriction should be overcome. To achieve this object, we investigated characteristics of ion-assisted aerosol lithography on a non-conducting substrate in Chapter 2. We found out that ion accumulation on nanoparticle structures caused termination of three-dimensional nanoparticle structure growth with scattered nanoparticles on a resist surface. Therefore, charge accumulation control on nanoparticle structures is the main key for successive growth of three-dimensional nanoparticle structures on a non-conducting substrate.

Up to date, ion-assisted aerosol lithography have been restrictively applicable to a non-conducting substrate as mentioned above. You et al. (2010) suggested ion-assisted aerosol lithography on a non-conducting substrate by employing a conducting liquid layer to conduct away the charges (Figure 3.1). However, for the formation of thin conducting liquid film, the substrate should have hydrophilic surface. In the case of hydrophobic surface, surfactant treatment should be required before nanoparticle deposition. Thus, complicating selection of substrate or additional preparation process is required for application of ion-assisted aerosol lithography on a non-conducting substrate.

Therefore, in this work, we suggested complemented method of ion-assisted aerosol lithography which can assemble three-dimensional nanoparticle structures on a non-conducting substrate without any restriction. At first, alternating electrode polarity was attempted to use accumulated charges inversely for assembly of charged nanoparticles on a non-conducting substrate. However, it was not enough to prevent

termination of three-dimensional nanoparticle structure growth on a non-conducting substrate. Based on the inadequacy of this approach, we suggested optimization of ion accumulation for the successful three-dimensional nanoparticle structure growth on a non-conducting substrate. Through the precise control of ion inflow using a corona discharger and an ion trap, various nanoparticle assembly results were obtained depending on the amounts of charge accumulation. Eventually, we have successfully demonstrated that the three-dimensional nanoparticle structure can be obtained by optimization of charge accumulation.

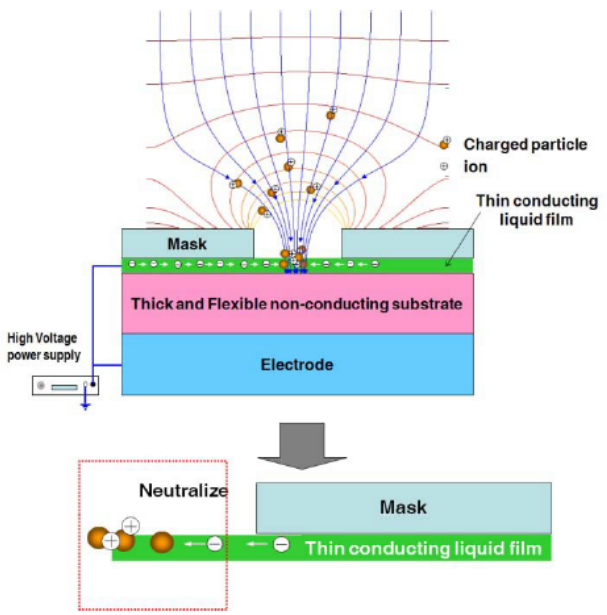

Figure 3.1. Schematic for patterning on a non-conducting substrate through formation of thin conducting liquid film (You et al. 2010)

3.2. Experimental concept

3.2.1. Polarity alternation to prevent termination of three-dimensional nanoparticle structure growth

In the Chapter 2, we found out that the charge accumulation on nanoparticle structures caused termination of three-dimensional nanoparticle structure growth. To prevent termination of three-dimensional nanoparticle structure growth, we attempt to alternate polarity of electrode voltage in deposition chamber.

Positively charged nanoparticles repelled from nanoparticle structures by electrical repulsion from the accumulated positive charges. However, we expected that accumulated positive charges can be work for attraction of nanoparticles if negatively charged nanoparticles are utilized as a building blocks of nanoparticle structures.

The pin-to-plated spark discharger generate bi-polar charged nanoparticles (Han et al. 2012). In the previous ion-assisted aerosol lithography method, only positively charged particles were used for the assembly because a negative potential was applied to the electrode for attraction of charged nanoparticle. On the other hand, if a positive potential is applied to the electrode, negatively charged particles can be attracted to a substrate, and it can be utilized to produce nanoparticle structures.

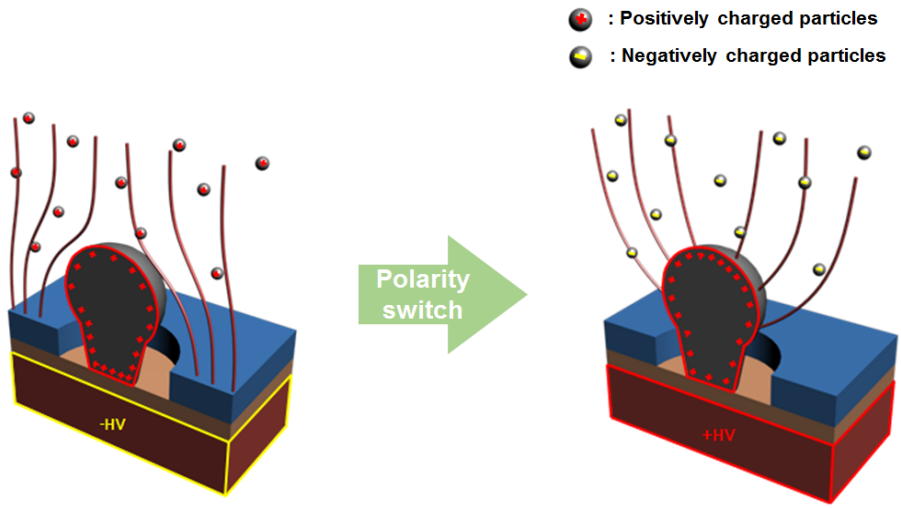

Figure 3.2. Strategy for three-dimensional nanoparticle structure growth by polarity alternation

Figure 3.2 shows strategy for three-dimensional nanoparticle structure growth by polarity alternation. When positive charges sufficiently accumulated on the nanoparticle structure, the electrode voltage alternates from negative to positive. Then, negatively charged particles attracted to a substrate and the accumulated positive charges in the nanoparticle structures can attract negatively charged particles. Therefore, we expected that three-dimensional structure can be obtained without repulsion of nanoparticles.

3.2.2. Selective capture of ions using the electrical mobility difference between nanoparticles and nitrogen ions

Another strategy for continuous growth of three-dimensional nanoparticle structure without termination is a control of ion inflow. The accumulated charges were originated from the two different sources; charged nanoparticles and ions. The charges of the nanoparticles were essential for ion-assisted aerosol lithography method, since it utilizes electric forces to control of particle movements. Therefore, accumulated charges should be controlled through the ion inflow manipulation.

To manipulate the ion inflow, we utilized electrical mobility difference between the Ag nanoparticles and nitrogen ions. Electrical mobility was defined as the ability of charged particles (or electrons or protons) to move through a medium in response to an electric field.

$$Z = \frac{V_{TE}}{\boldsymbol{E}} \tag{3.1}$$

where, Z is electrical mobility, V_{TE} is terminal velocity, and E is magnitude of the applied electric field. In the Stokes region, the terminal velocity V_{TE} is obtained by equating the electrostatic force to Stokes drag and solving for velocity.

$$ne\boldsymbol{E} = \frac{3\pi\mu V d}{C_c} \tag{3.2}$$

$$V_{TE} = \frac{neEC_c}{3\pi\eta d} \tag{3.3}$$

where, n is charge number, e is electric constant, μ is viscosity, and C_c is *Cunningham correction factor* (Eq. 2.5). Thus, the electrical mobility of charged particles (or electrons) is

$$Z = \frac{V_{TE}}{E} = \frac{neC_c}{3\pi\mu d} \tag{3.4}$$

Table 3.1 shows electrical mobility of electrons, and ions and aerosol particles at standard conditions (Hinds, 1999). Therefore, the electrical mobility of positive ions is 10^2 times larger than that of few nanometers of singly charged nanoparticle.

Table 3.1 Electrical mobility of electrons, ions, and aerosol particles at standard conditions (Hinds, 1999)

Particle Diameter (μm)	Electrical Mobility ($m^2/V \cdot s$)[a]	
	Singly Charged	Maximum Charge[b]
Electron	6.7×10^{-2}	-
Negative air ion	1.6×10^{-4}	-
Positive air ion	1.4×10^{-4}	-
0.01	2.1×10^{-6}	7.3×10^{-4}
0.1	2.7×10^{-8}	9.3×10^{-4}
1.0	1.1×10^{-9}	$(2.5 \times 10^{-3})^c$
10	9.7×10^{-11}	$(6.7 \times 10^{-3})^c$
100	9.3×10^{-12}	$(1.1 \times 10^{-2})^c$

[a]For mobility in $cm^2/stV \cdot s$, multiply the value shown by 3×10^6

[b]Based on the ion limit

[c]Velocity (m/s) in a unit electric field, but because Re > 1.0, Eq. 3.3 does not hold

Ion trap was designed for selective capture of electrons by utilizing electrical mobility difference between the Ag nanoparticle and the ion. An electrode was installed at the tube which the charged Ag nanoparticles and positive nitrogen ions were passed (Figure 3.3a).

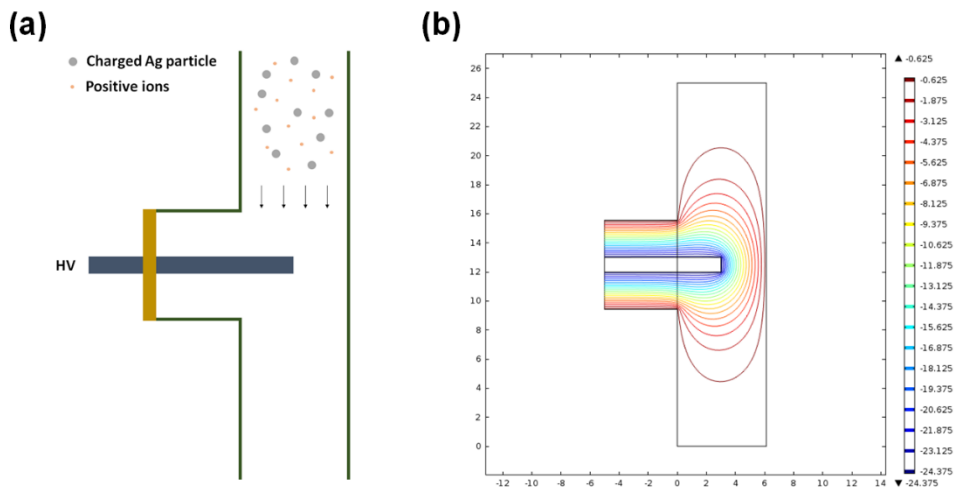

Figure 3.3. (a) Structure of the ion trap for selective capture of ions. (b) Electric field simulation results at the ion trap electrode

By applying ion trap voltage to the electrode, charged Ag nanoparticles and positive ions are attracted to the electrode as shown at Figure 3.3b. Since the nanoparticles and ions have different electrical motilities, there are certain voltage which enable only nitrogen ions are captured whereas the charged Ag nanoparticles cannot.

3.3. Experimental method

3.3.1. Particle generation

Ag nanoparticles which have 4.3 nm geometric mean diameter were generated by pin-to-plate spark discharger (Han et al. 2012). The spark discharger conditions were same as Chapter 2 (resistivity: 10 MΩ, capacitance: 2 nF, nitrogen gas flow: 1 lpm and applied voltage 4.5 kV). A corona discharger with 3.5 kV (HV2 of Figure 2.5a) applied to its electrode and 1 lpm nitrogen flow was used for addition of ions.

Particle size distribution is shown at Figure 3.4 which was measured using the scanning mobility particle sizer (SMPS, Model 3080, TSI Inc., USA) system which was comprised of a neutralizer (Model 3077, TSI Inc., USA), a differential mobility analyzer (Model 3085, TSI Inc., USA), and a condensation particle counter (Model 3776, TSI Inc., USA).

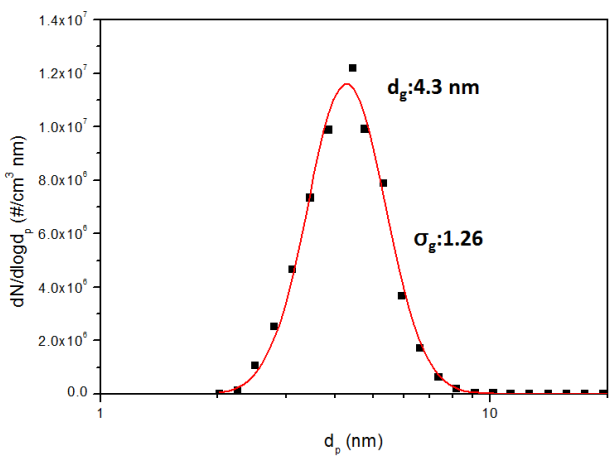

Figure 3.4. Particle distribution of Ag nanoparticles which was generated from pin-to-plate spark discharger

3.3.2. Assembly of charged nanoparticles on a non-conducting substrate by using polarity alternation

First, we attempt to alternate polarity for continuous growth of three-dimensional nanoparticle structures. The experimental set-up is same as the Figure 2.5a. Before 60 minute of deposition time, positively charged Ag nanoparticles are dragged to substrate with electrode voltage at -2.0 kV (HV3 of Figure 2.5a). The electrode voltage was alternated from – 2 kV to + 2 kV at 60 minutes which is a time that sufficient charges could be accumulated on nanoparticle structures. It means that negatively charged nanoparticles are attracted to substrate after that 60 minutes of deposition times. Thus, negatively charged nanoparticles are used to produce nanoparticle structures as a building block after 60 minutes while the positively charged nanoparticles are used before 60 minutes.

3.3.3. Optimization of ion inflow by the ion trap

Figure 3.5 shows experimental set-up for the three-dimensional nanoparticle growth optimization on a non-conducting substrate by ion inflow control. Ion trap was installed at the inlet of deposition chambers for the precise control of ion inflow.

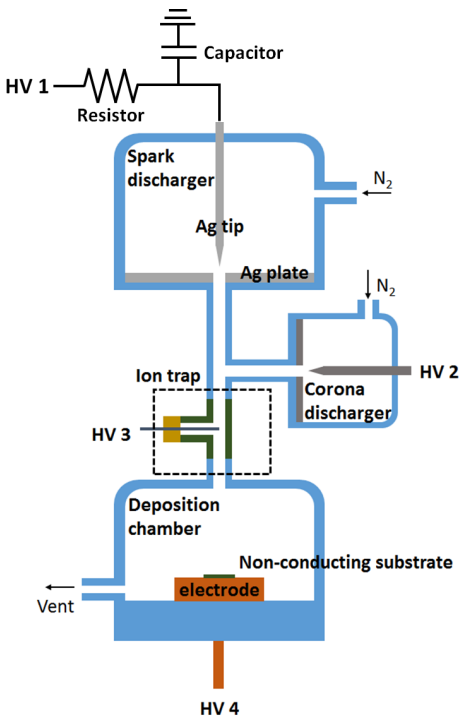

Figure 3.5. Experimental set-up for the three-dimensional nanoparticle growth optimization on a non-conducting substrate by ion inflow control

First of all, the performance of the ion trap was evaluated. The ion inflow was measured by Faraday cup electrometer. The total particle concentration was measured by SMPS (Model 3080, TSI Inc., USA) system which was comprised of a neutralizer (Model 3077, TSI Inc., USA), a differential mobility analyzer (Model 3085, TSI Inc., USA), and a condensation particle counter (Model 3776, TSI Inc., USA).

Secondly, we fabricated the three-dimensional nanoparticle structures without termination by optimizing ion inflow. The corona discharger and ion trap were used to control of ion inflow. In the spark discharger, charged nanoparticles and nitrogen ions were generated. Optionally, nitrogen ions generated from the corona discharger can be added to the out stream of the spark discharger. Finally, precise control of the ion inflow was conducted by adjusting the ion trap voltage with 0-20 V. To compare the ion inflow among the experimental conditions, a Faraday cup electrometer was used to measure total currents which were caused from both charged nanoparticles and ions. Through comparison of the total current values, we could obtain relative comparison of the ion inflow because the measured current from the nanoparticles was fixed.

The results of nanoparticle assembly on a non-conducting substrate were observed using field-emission scanning electron microscopy (FE-SEM, Merlin Compact, Carl Zeiss, Oberkochen, Germany) at an acceleration voltage of 2 kV.

The electric field simulation was conducted for understanding of experimental results by using electrostatic modules of COMSOL Multiphysics 4.4.

3.4. Results and discussion

3.4.1. Assembly of three-dimensional nanoparticle structures by using polarity alternation

Figure 3.6 shows experimental results for three-dimensional nanoparticle structure growth on a non-conducting substrate with/without a polarity alternation. The repulsion of incoming particles were not observed when the nanoparticle structure was assembled with polarity alternation and nanoparticle structures were enlarged than that of the case without polarity alternation. However, many noise particles were observed on a resist surface as shown at Figure 3.6b. To elucidate this experimental results, electric field results was conducted

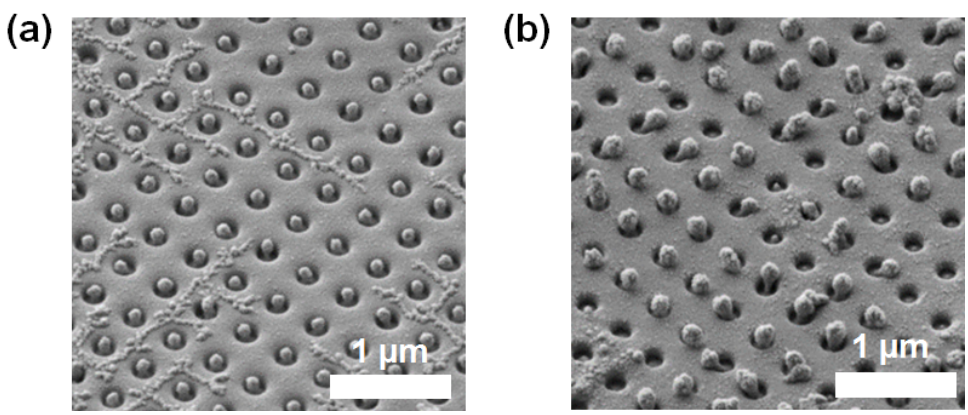

Figure 3.6. SEM images of three-dimensional nanoparticle structure growth on a non-conducting substrate (a) without polarity alternation and (b) with polarity alternation. The electrode voltage was alternated from – 2.0 kV to +2.0 kV at 60 minutes of deposition time

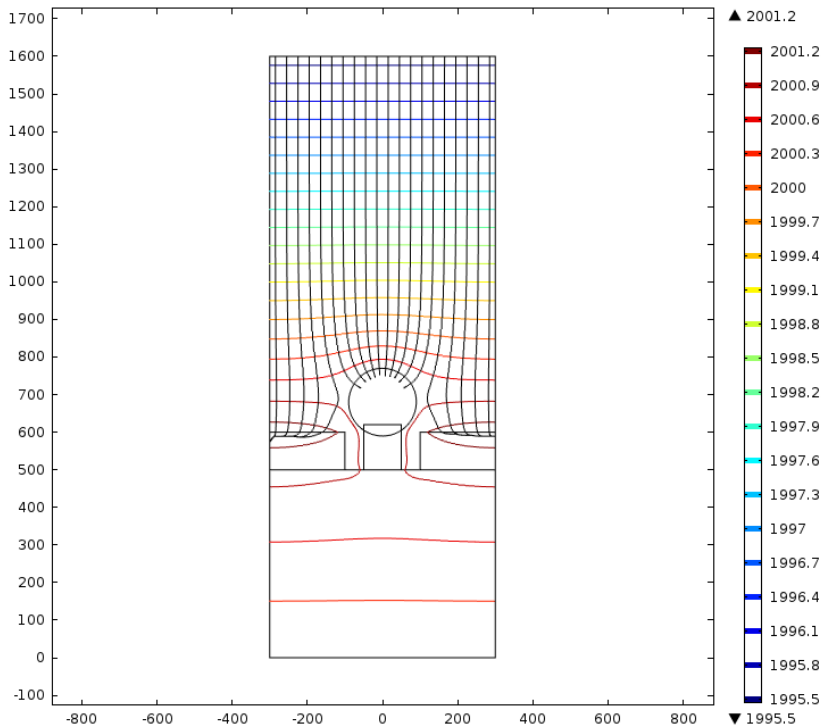

Figure 3.7. Electric field simulation results when the electrode voltage was alternated from -2.0 kV to +2.0 kV

Figure 3.7 shows electric field simulation results when the electrode voltage was alternated from -2.0 kV to +2.0 kV. When the electrode voltage was alternated from negative to positive, accumulated charges in the positive charges attracted negatively charged nanoparticles as we expected. However, the repulsive force from accumulated charges in resist surface was removed by the polarity alternation. As a result, only negatively charged nanoparticles at nearby the nanoparticle structure were dragged to the nanoparticle structures, whereas the negatively charged nanoparticle at far from the structures were dragged to the resist surface. From the results, we can demonstrate that electrical repulsion between charged nanoparticles

and accumulated charges on resist surface was necessary for fabrication of three-dimensional nanoparticle structure even though attractive forces existed between the nanoparticle structure and incoming particles. Thus, for the continuous growth of three-dimensional nanoparticle structure, we should induce attractive force between the nanoparticle structure and incoming particles (green arrows in Figure 3.8) and also induce repulsive force between accumulated charges on the resist surface and incoming particles (red arrows in Figure 3.8). Therefore, polarity alternation of electrode voltage is not enough to three-dimensional nanoparticle structure growth on a non-conducting substrate.

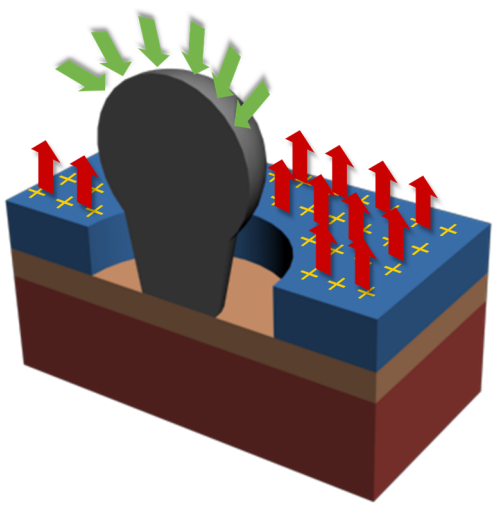

Figure 3.8. Schematic for force balance during growth of three-dimensional nanoparticle structure

3.4.2. Selective capture of ions by using ion trap

Figure 3.9 shows the performance of the ion trap depending on the ion trap voltages. We applied 0-25 V to the ion trap electrode and calculated ion transmission ratios, which was defined as the ratio of the current measured when the ion trap was on to the current measured when the ion trap was off.

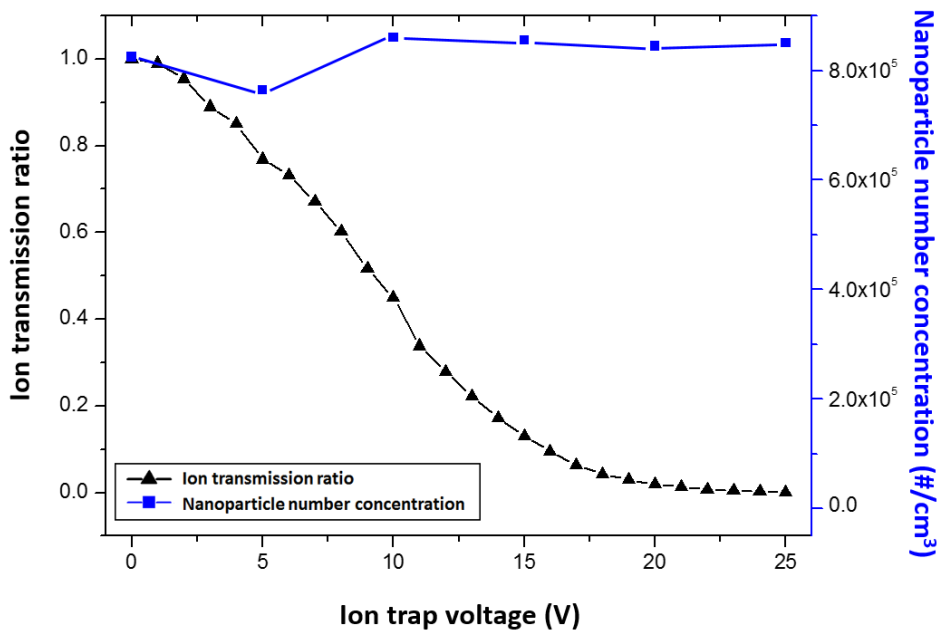

Figure 3.9. Performance evaluation of ion trap in the rage of voltages from 0 V to 25 V

Ion transmission ratio can be varied from 1 to almost nothing (less than 0.02) by increasing the voltage applied to the ion trap electrode from 0 to 25 V. The total number of nanoparticles reaching the deposition chamber does not changed significantly over this ion trap voltage range. Therefore, the ion trap enables a precise control of the ion inflow over a wide range during nanoparticle assembly process.

3.4.3. Assembly of three-dimensional nanoparticle structures by optimization of ion inflow

Fig.3.10 shows the results of three-dimensional nanoparticle structure growth depending on the ion inflow. The results were arranged in the descending order of the ion inflow. The experimental conditions of each cases was shown at Table 3.2, arranged in descending order of ion inflow indicated by measured current.

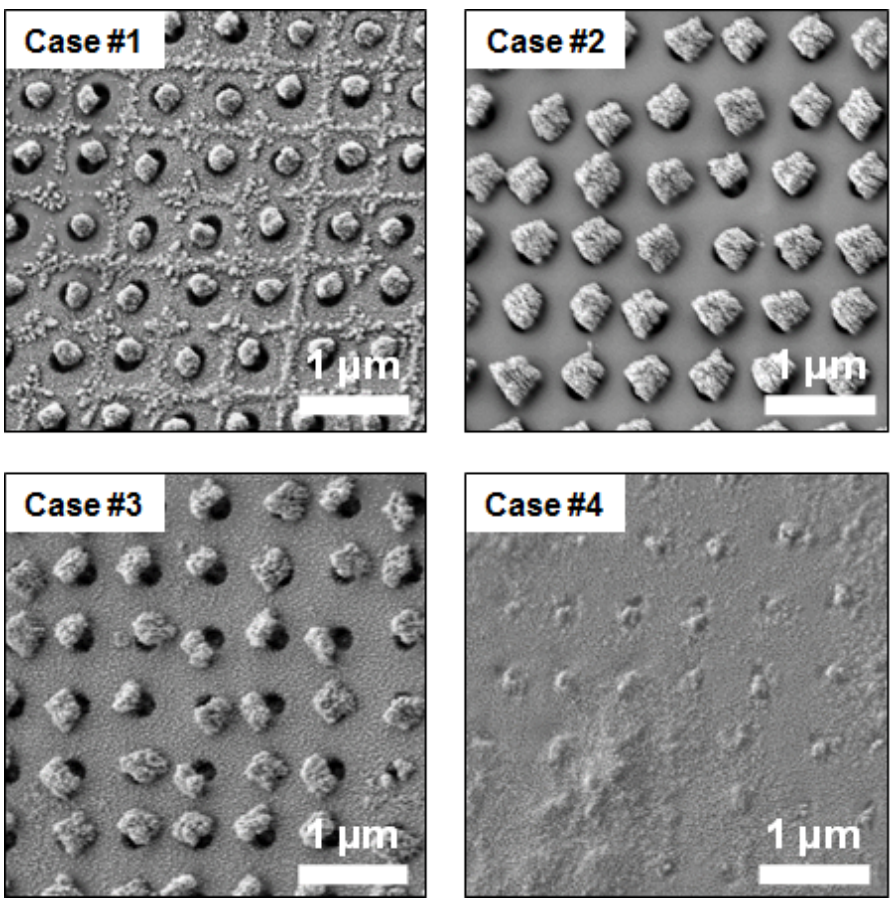

Figure 3.10. SEM images of three-dimensional nanoparticle structures depending on the ion inflow

Table 3.2. Experimental conditions for ion-assisted aerosol lithography on a non-conducting substrate with adjusted ion flow

	Corona discharger	Ion trap voltage (V)	Measured current (pA)
Case #1	ON	0	10.1
Case #2	ON	5	7.9
Case #3	OFF	0	3.5
Case #4	OFF	20	2.3

Figure 3.11 shows the results of the electric field simulation of each cases. When the excessive ions were injected, too many charges were accumulated in the nanoparticle structures. As a result, repulsive forces were applied to the nanoparticles from the accumulated charges within the structures (Case #1, measured current: 10.1 pA). Otherwise, when a very small amount of ions were injected into the deposition chamber, the nanoparticles were deposited all over the substrate without assembling into three-dimensional nanoparticle structures (Case #4, measured current: 2.3 pA) as there weren't enough ions on the resist surface to induce electrostatic lens effect. In Case #3 (Measured current: 3.5 pA), the nanoparticle structures were assembled by the electrostatic lenses with a lot of noise nanoparticles on a resist surface. It is because the ion build-up on the resist surface was not enough to prevent nanoparticle deposition on it. For Case #2 (Measured current: 7.9 pA), three-dimensional nanoparticle structure growth was successfully assembled without unwanted nanoparticle deposition elsewhere. This set of conditions provided enough ions to be deposited on the resist surface to prevent nanoparticle deposition and induce

electrostatic lens effect, yet kept the charge accumulation within nanoparticle structures to levels that allowed continuous growth without terminating up until 120 minutes. From these results, it is evident that assembling nanoparticle structures via ion-assisted aerosol lithography on a non-conducting substrate takes more delicate tuning of the experimental conditions, where the strength of electrostatic lens effect and the amount of charge build-up within the structures should be carefully balanced for optimized nanoparticle structure growth.

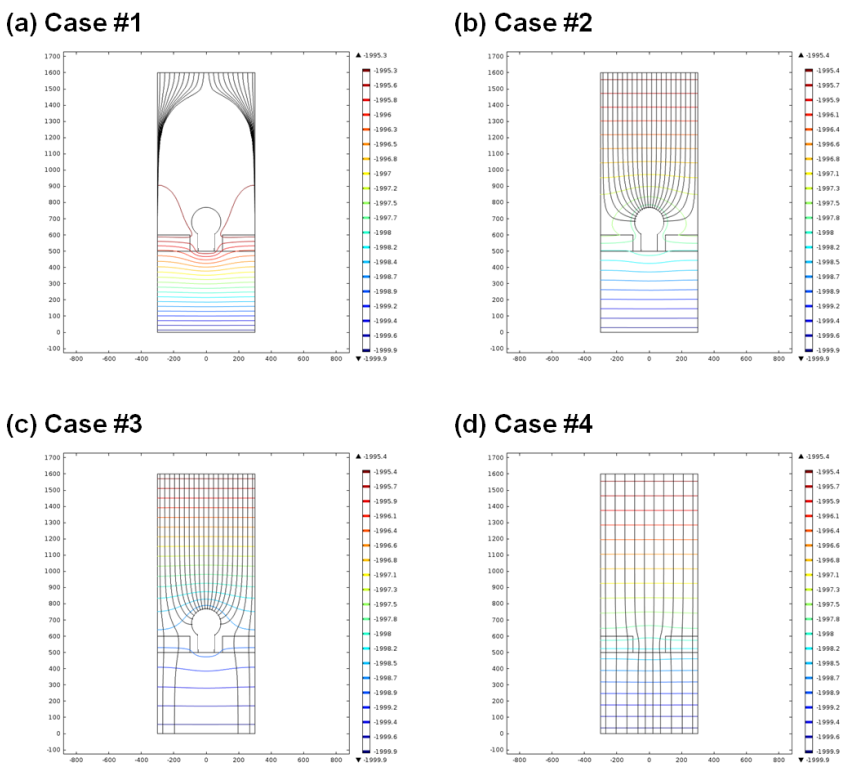

Figure 3.11. Electric field simulation results of nanoparticle structure growth on a non-conducting substrate depends on the ion inflow

Figure 3.12 shows cross section images of the three-dimensional nanoparticle structures on a non-conducting substrate which was measured by focused ion beam scanning electroscope (FIB-SEM). It shows successful growth of mushroom-like three-dimensional nanoparticle structures on a non-conducting substrate. However, each nanoparticle structures have slightly different shapes. The non-uniformity of the nanoparticle structures was originated from the weak electric field strength than the case of the conducting substrate. The non-uniformity of the nanoparticle structures are getting worse as the growth of nanoparticle structures (Figure 2.8). When the nanoparticle structures was grown over the resist pattern, the non-uniformity was critically increased because the spatial restriction of incoming charged nanoparticles was removed. Therefore, the non-uniformity problem can be solved by using the nanoparticle structure if the structure is not over the resist pattern.

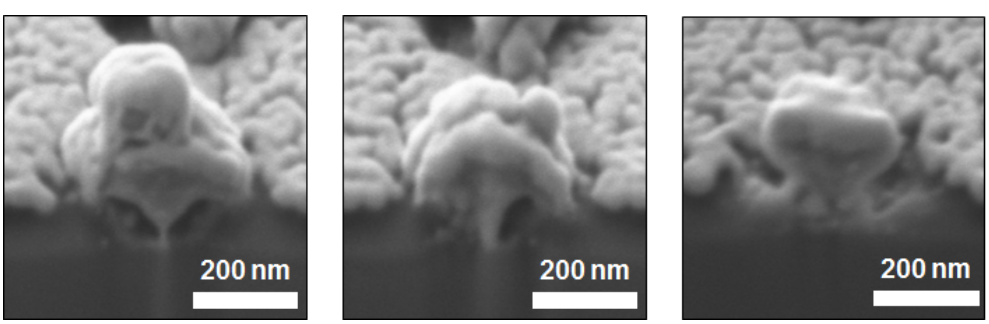

Figure 3.12. Cross section images of the three-dimensional nanoparticle structures on a non-conducting substrate

Figure 3.13 shows three-dimensional nanoparticle structure growth on a non-conducting substrate which have 2 μm diameter and 1 μm thickness hole resist pre-pattern. The results show uniform three-dimensional nanoparticle structure on a non-conducting substrate. Thus, the uniform three-dimensional nanoparticle structures which have desired size can be obtained by modifying geometry of resist pre-pattern. The amount of ion inflow was easily optimized by a corona discharger and an ion trap at the new condition (Corona discharger: On, Ion trap voltage: 0 V).

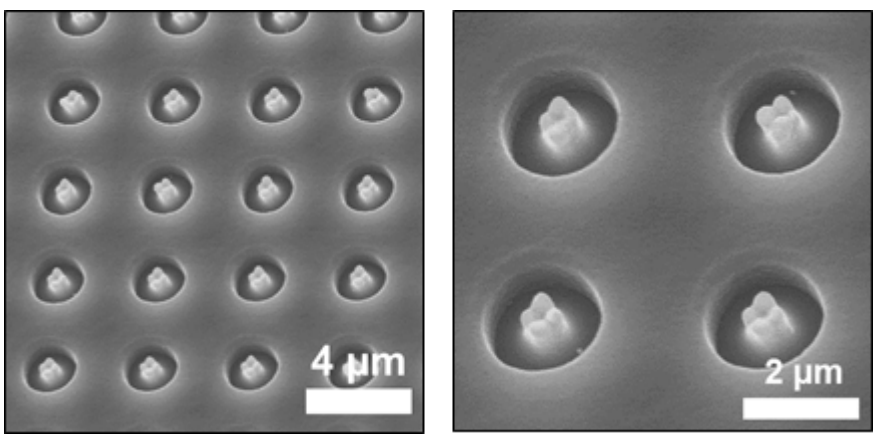

Figure 3.13. Three-dimensional nanoparticle structures on a non-conducting substrate which have 2 μm hole resist pre-pattern

3.5. Conclusion

In this research, we adequately optimized the charged nanoparticle structure growth process via ion-assisted aerosol lithography on a non-conducting substrate. In the Chapter 2, we found that ion-assisted aerosol lithography on a non-conducting substrate is much more challenging compare to the conducting substrate due to the fact that charges are remained on the nanoparticle structures which eventually leads to termination of the nanoparticle assembly process. By using a corona discharger and an ion trap, we verified that the ions can be selectively added or removed from the stream without affecting the quantity of nanoparticles. Through this capability, the amount of ion inflow was manipulated to a level that generates electrostatic lens effect without excessive charge build-up that repels incoming nanoparticles after a prolonged deposition of 120 minutes. Consequently, we successfully obtained the three-dimensional nanoparticle structures on a non-conducting substrate through optimization of ion inflow. These findings confirm that the role of electric field distortion is critical in architecting the three-dimensional nanoparticle structures, and not only expands the versatility of the ion-assisted aerosol lithography process to non-conducting substrates, but also opens up an opportunity to create more complex three-dimensional nanoparticle architectures by regulating the charge build-up and/or electric field distortions during the ion-assisted aerosol lithography process in general.

Chapter 4.

Large area assembly of charged nanoparticles on a non-conducting substrate via electrified mask

4.1. Introduction

High-resolution array of nanoparticles can be obtained without any damages of substrate via ion-induced focusing mask (You et al. 2010). Since the electrostatic lenses are generated on the floated mask which is separated from the substrate, the electrostatic lenses can be translated relatively to the substrate. Therefore, high density of nanoparticle assembly array can be obtained through sequential operation with translation of the mask, and focusing mask can be used repeatedly since the nanoparticles are selectively deposited onto the substrate, not on the mask, which eliminates the need to prepare a new mask for each operation.

Electrified mask is advanced form of ion-induced focusing mask (Choi et al. 2015). In this method, electrostatic lenses are generated by applying an electric potential to metal coated stencil mask. Therefore, electrified mask not only has advantages of ion-induced focusing mask, but also it has another great advantage which is precise control of electrostatic lenses by adjusting applied potential. However, the electrified mask method on a non-conducting substrate has not been sufficiently investigated which means that it has been limited to a conducting substrate. Fortunately, this method has additional benefit for application to a non-conducting substrate. In the previous work at Chapter 2 and 3, we figured out that ion accumulation is a main parameter of charged nanoparticle assembly on a non-conducting substrate, and we showed that three-dimensional nanoparticle structures on a non-conducting substrate could be obtained through optimization of ion accumulation. In the electrified mask method, ions are not needed anymore because this method utilize electric potential of mask surface to generate electrostatic lens, not the ion accumulation.

Here, we performed a study about development of electrified mask method for the practical use of it in the two respects. First, large area assembly system was designed

through large area polymer electrified mask and multi-spark discharger. Second, we presented that nanoparticle assembly on a thick non-conducting substrate could be obtained by elimination of ion injection. Consequently, we demonstrated that large area charged particle assembly on a thick non-conducting substrate can be achieved via advanced electrified mask system.

4.2. Experimental concept

4.2.1. Controlled electrostatic focusing of charged nanoparticles via an electrified mask

High-resolution array of nanoparticles can be obtained without any damages of target substrate by using ion induced focusing mask (You et al. 2010). Charged nanoparticles are guided into desire position through the electrostatic lens which is produced by accumulated ions on focusing mask (Figure 4.1a). High density of nanoparticle assembly array can be obtained through the translation of focusing mask (Figure 4.1b and c).

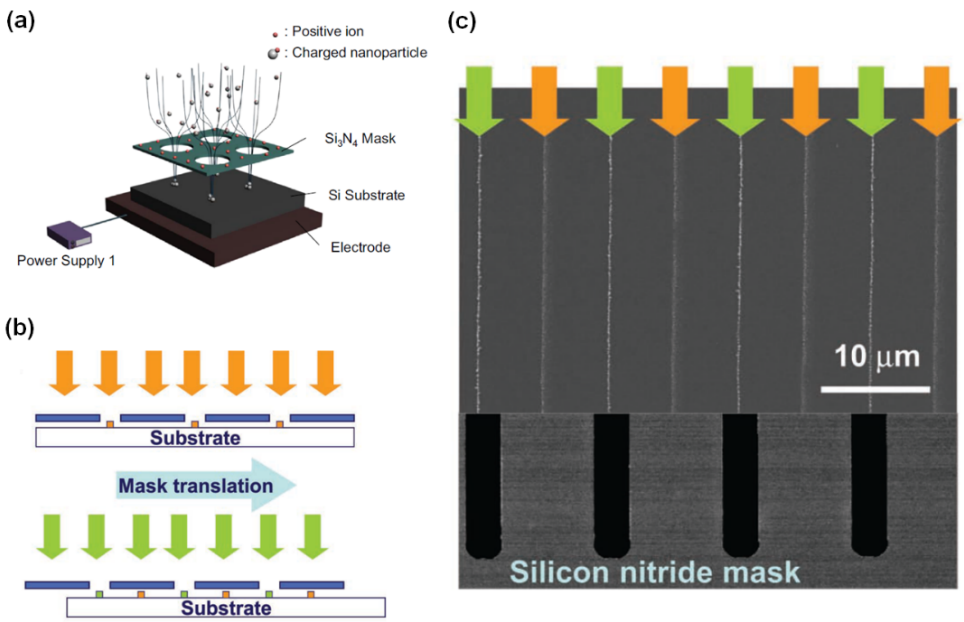

Figure 4.1. Schematic for (a) nanoparticle assembly method by using ion induced focusing mask (Choi et al. 2015) and (b) Sequential operation of the ion-induced focusing mask. (c) SEM images of sequential patterning through translation of the mask (You et al. 2010)

Because the ion-induced focusing mask have a distance from the substrate, the electrostatic lenses can be translated relatively without any disturbance, whereas the ion-assisted aerosol lithography that using resist pattern cannot. In addition, this mask can be used repeatedly since the nanoparticles are selectively deposited onto the substrate, not on the mask, which eliminates the need to prepare a new mask for each operation.

The ion-induced focusing mask was progressed to electrified mask which enable precise control of focusing ratio (Choi et al. 2015). In the electrified mask method, electric potential on a metal layer of mask is used for generation of electrostatic lenses (Figure 4.2a). Unlike ion-induced focusing mask, the electrostatic lens can be controlled by manipulation of electric potential on the mask surface in electrified mask method. Therefore, the size of nanoparticle assembly can be controlled precisely as shown at Figure 4.2b.

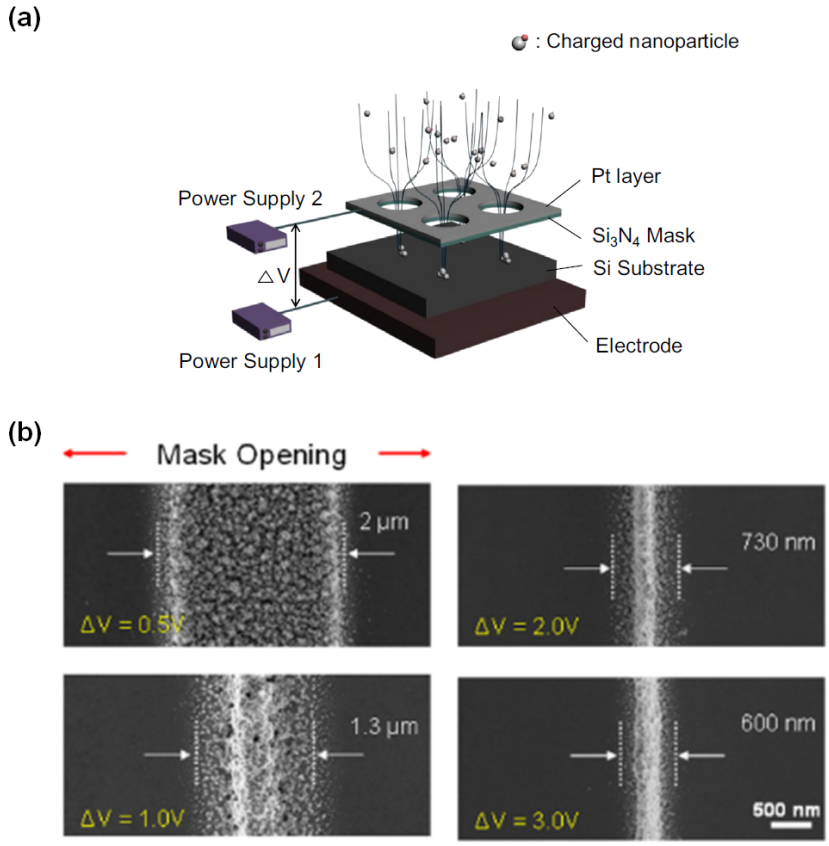

Figure 4.2. (a) Schematic representations of nanoparticle assembly method by voltage difference between the substrate and electrified mask. (b) Effect of the potential difference on the pattern width (Choi et al. 2015)

4.2.2. Design of a large area nanoparticle assembly system through multi-spark dischargers and a polymer electrified mask

For a large area nanoparticle assembly system, we considered two main part of the system; particle spray part and particle deposition part (Figure 4.3). At first, we used multi-spark discharger system to uniform spray of nanoparticles. The nanoparticles from the multi-spark discharger was electrically attracted to a large area polymer electrified mask. Then, the charged nanoparticles were focused into center of the electrified mask opening by electrostatic lenses.

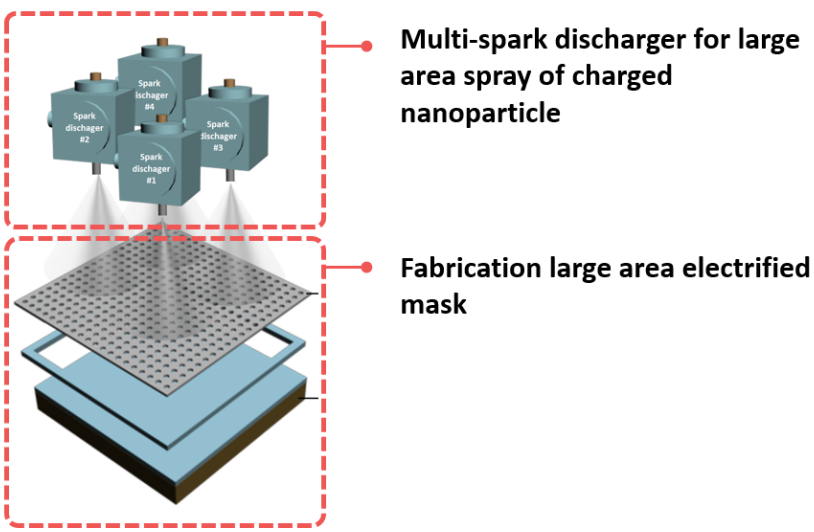

Figure 4.3. Strategy for large area nanoparticle assembly system through the multi-spark discharger and the large area electrified mask

Move on the particle deposition part, a large area electrified mask was needed for the large area particle deposition system. In previous electrified mask research, electrified mask was fabricated using silicon nitride which have strong mechanical strength in the size of few hundreds micrometer scale. However, when the silicon nitride mask produced in large area, it was easily break. To secure strength of enhanced patterning area of the electrified mask, we designed polymer electrified mask which have thicker and larger size of apertures than the silicon nitride mask. An effect of mask thickness was considered through electric field simulation (Figure 4.4). It shows that thick electrified mask disturb generation of the electrostatic lens. It is because the thick mask reduces spatial difference of electric potential which makes electrostatic lens formation.

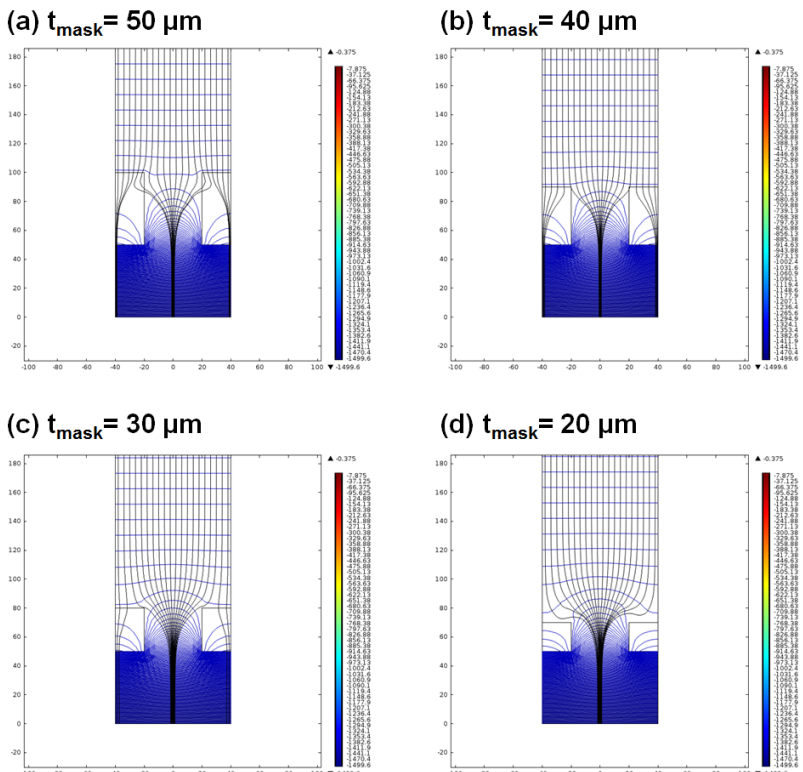

Figure 4.4. Electric field simulation results for effect of mask thickness

Therefore, we used 20 μm thickness of polymer stencil for the large area electrified mask (Figure 4.5a). The large area polyurethane acrylate (PUA) polymer stencil which have 40 μm opening (40 μm spacing) was easily obtained from the polydimethylsiloxane (PDMS) mold via soft lithography. The size of polymer mask was 3 cm x 3 cm. Pt sputter was used to deposition of Pt layer on the polymer stencil surface.

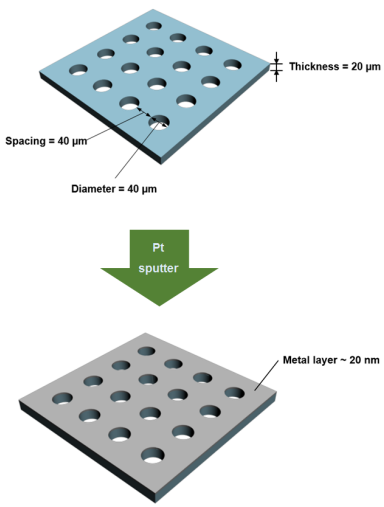

Figure 4.5. Structure of the electrified mask using large area polymer stencil

4.2.3. Assembly of charged nanoparticles on a non-conducting substrate through elimination of ions and a polymer electrified mask

Assembly of charged nanoparticle via electrified mask enable precise control of electric potential at the mask surface. Therefore, the focusing ratio can be easily controlled by adjusting mask potential. Not only that, electrified mask have great advantages when it applied to a non-conducting substrate. In the previous Chapter, we found out that the ion accumulation is a key parameter of charged nanoparticle assembly on a non-conducting substrate. Because the electrified mask methods can generate electrostatic lenses without ions, it is very useful method for nanoparticle assembly on a non-conducting substrate. Figure 4.6 shows strategy of charged nanoparticle assembly on a non-conducting substrate via electrified mask.

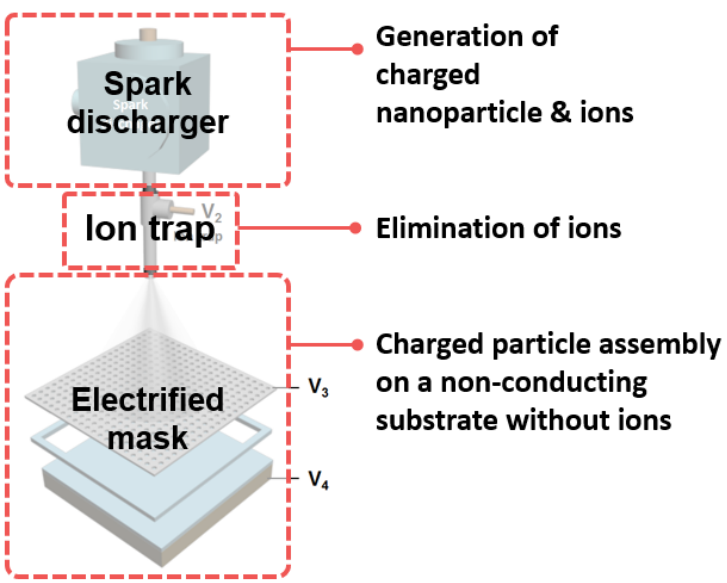

Figure 4.6. Strategy of charged particle assembly on a non-conducting substrate via electrified mask

Spark discharger necessarily generate ions as by-product of charged nanoparticles. The ion trap is installed at the out flow of the spark discharger for elimination of ions. In Chapter 3, we show that ions could be selectively captured without any changes of particles. Therefore, only charged nanoparticles can arrive at the electrified mask. The charged nanoparticles can be assembled through electrified mask without ions.

4.3. Experimental method

4.3.1. Particle generation

The experimental set-up for large area assembly of charged nanoparticles on a non-conducting substrate was shown at Figure 4.7a. The wire-in-hole spark discharger was used for generation of Cu nanoparticles which have 5.1 nm geometric mean diameter (Chae et al. 2014). The 10 MΩ resistors and 2 nF capacitors were used for the spark circuit. The 2 lpm of nitrogen flow was used for the carrier gas. Figure 4.7b shows particle distribution of Cu nanoparticles from the spark discharger. Particle size distribution was measured using the scanning mobility particle sizer (SMPS, Model 3080, TSI Inc., USA) system which was comprised of a neutralizer (Model 3077, TSI Inc., USA), a differential mobility analyzer (Model 3085, TSI Inc., USA), and a condensation particle counter (Model 3776, TSI Inc., USA). Multi-spark dischargers was utilized for large area assembly of the charged nanoparticles.

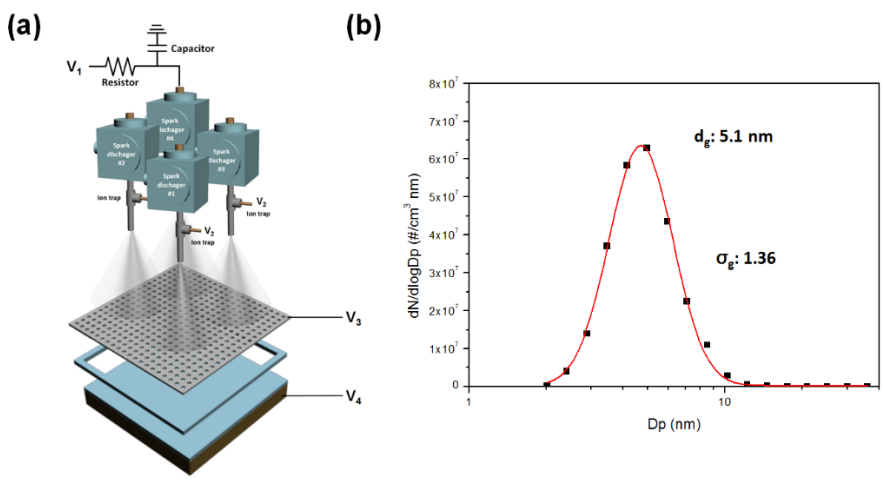

Figure 4.7. (a) Experimental set-up for large area nanoparticle assembly via electrified mask. (b) Particle distribution of Cu nanoparticle which was generated from the wire-in-hole spark discharger in this experiment

4.3.2. Charged nanoparticle assembly via large area electrified mask

The metal coated polymer mask was located on the PET spacer which have 50 μm of thickness (Figure 4.8). Since the sputter have good step coverage, the Pt layer was also deposited on the side wall of the opening. Therefore, the spacer should be required to prevent electrical contacting between the electrode and the metal layer on the polymer mask. If the metal layer on the polymer mask contacted to the substrate, the electrostatic focusing is impossible because the electric potential of the metal layer became equal to the electric potential of the electrode. Therefore, the four sides of the polymer mask should be pulled tight and fixed to minimize sagging of it.

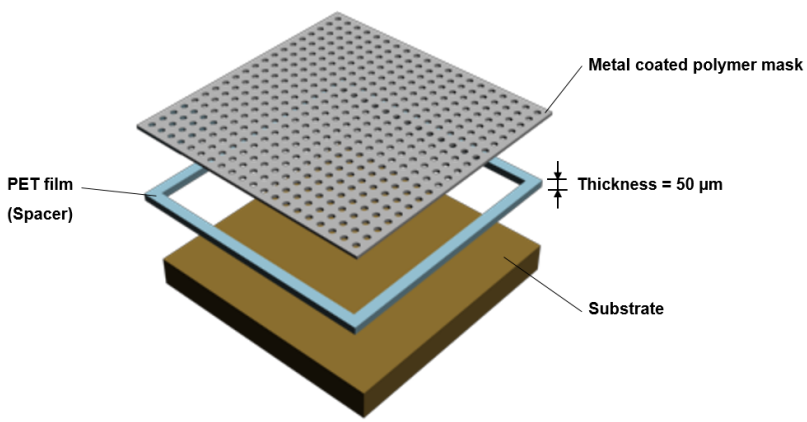

Figure 4.8. Schematic representation of nanoparticle assembly by using metal coated polymer mask

When the nanoparticle structures fabricated on a non-conducting substrate, nitrogen ions were selectively captured by ion traps. -25.0 V voltage was applied to the ion trap electrode for elimination of the ions (Figure3.8). Glass substrate which have 1 mm thickness was used as a non-conducting substrate.

The results of nanoparticle assembly were observed using field-emission scanning electron microscopy (FE-SEM, Merlin Compact, Carl Zeiss, Oberkochen, Germany) at an acceleration voltage of 2 kV.

4.3.3. Determination of electric potential values at the electrified mask surface

The electric field was calculated using electrostatic modules of COMSOL multiphysics 4.4 for determination of electric potential values at the electrified mask surface. The electric field simulation was conducted with a square area of 80 μm × 20000 μm. The area covered one single pattern width and whole height from substrate to particle inlet (Figure 4.9).

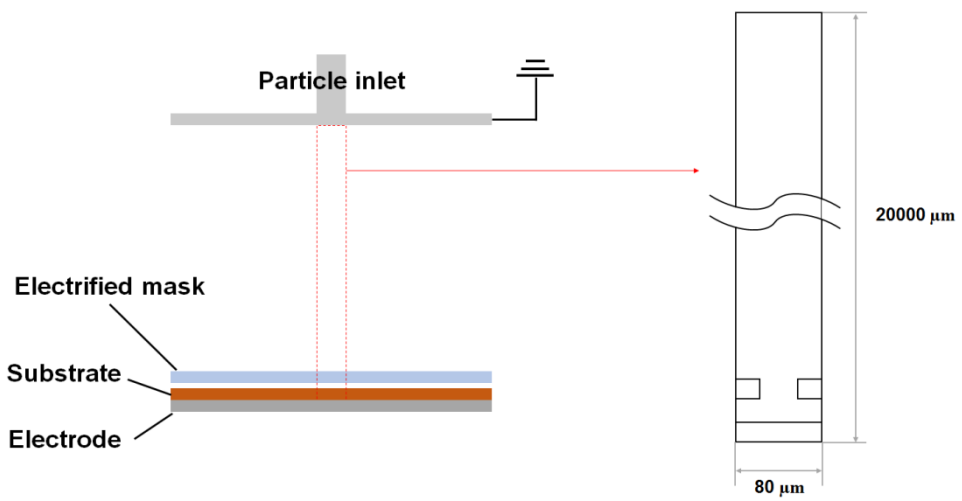

Figure 4.9. The electric field simulation area for assembly of charged nanoparticles via electrified mask

When potential values on electrified mask was determined, breakdown voltage should be considered to avoid discharge between a substrate and a mask. Breakdown voltage can be calculated by Paschen's law (Burm 2007).

$$V_B = \frac{Bpd}{\ln(Apd) - ln\left(ln\left(1 + \frac{1}{\gamma}\right)\right)} \tag{4.1}$$

where p is a pressure, d is a gap distance, A and B are constant, and γ is Townsend coefficient. The coefficient of Eq.4.1 is shown at Table 4.1. The breakdown voltage between the substrate and the electrified mask is calculated to about 512 V in our experimental condition. Therefore, experiments were conducted with potential difference below 400 V.

Table 4.1. Paschen coefficients for several commonly used gases (Burm 2007)

gas	A $[Pa^{-1}m^{-1}]$	A [V $Pa^{-1}m^{-1}$]	γ
He	2.10	25.50	0.263
N_2 (air)	10.95	273.78	0.025
Ar	10.20	176.27	0.095

4.4. Results and discussion

4.4.1. Large area assembly of charged nanoparticles via electrified mask

Before the assembly of charged nanoparticles on a non-conducting substrate, we performed large area assembly of charged nanoparticles on a conducting substrate via polymer electrified mask. Figure 4.10 shows polymer mask for the large area assembly of charged nanoparticles. 3 cm × 3 cm size of polymer mask was obtained from soft lithography. The polymer mask have 40 μm opening (40 μm spacing) and 20 μm thickness as shown at Figure 4.10. The large area electrified mask was obtained by coating Pt layer on the polymer mask. Then, the charged Cu nanoparticles from multi-spark discharger was sprayed on the large area electrified mask.

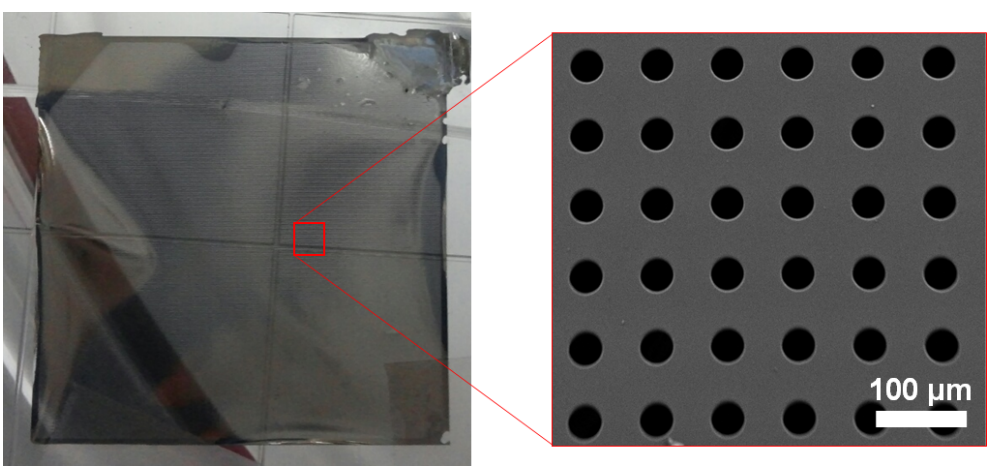

Figure 4.10. Polymer mask for large area assembly of charged nanoparticles

Electrical potential values at the mask surface was obtained from electric field simulation results (Figure 4.11). The electric field simulation results shows that electrostatic lens is well generated when 200 V of potential difference was applied between the electrode and the electrified mask.

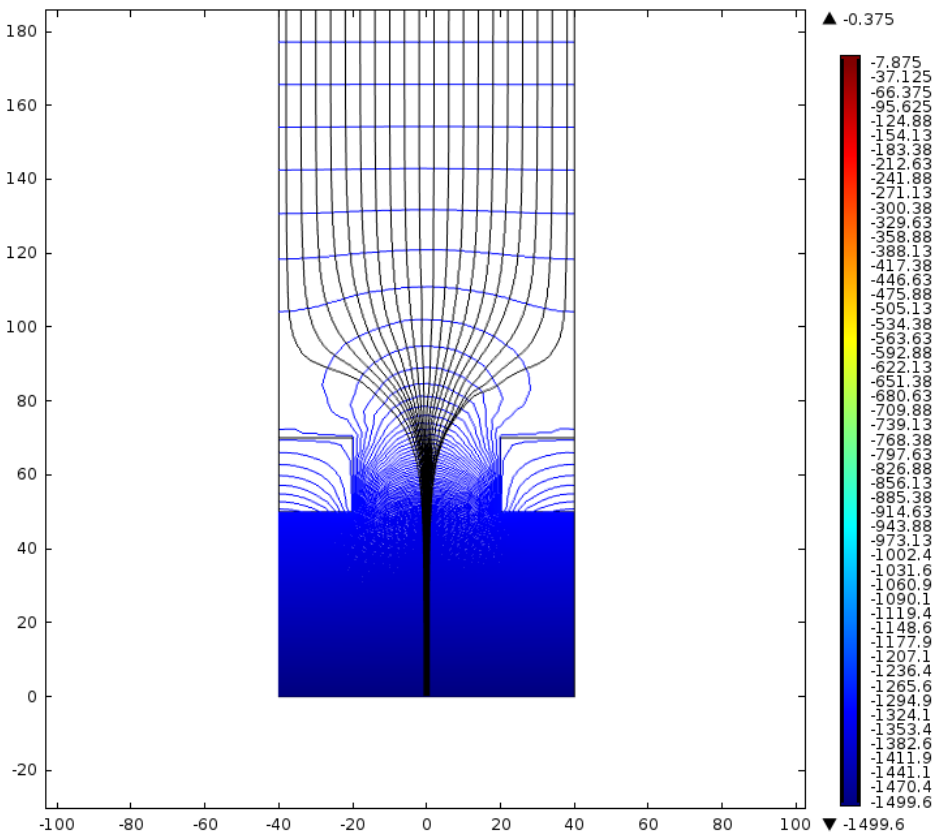

Figure 4.11. Electric field simulation results when 200 V of electric potential difference was applied between the electrode and the electrified mask

For the large area assembly of charged nanoparticles, large area polymer electrified mask and multi-spark discharger were used in order to generate large area electrostatic lenses and large area spray of charged nanoparticles, respectively. The results for large area assembly of charged nanoparticles are shown at Figure 4.12.

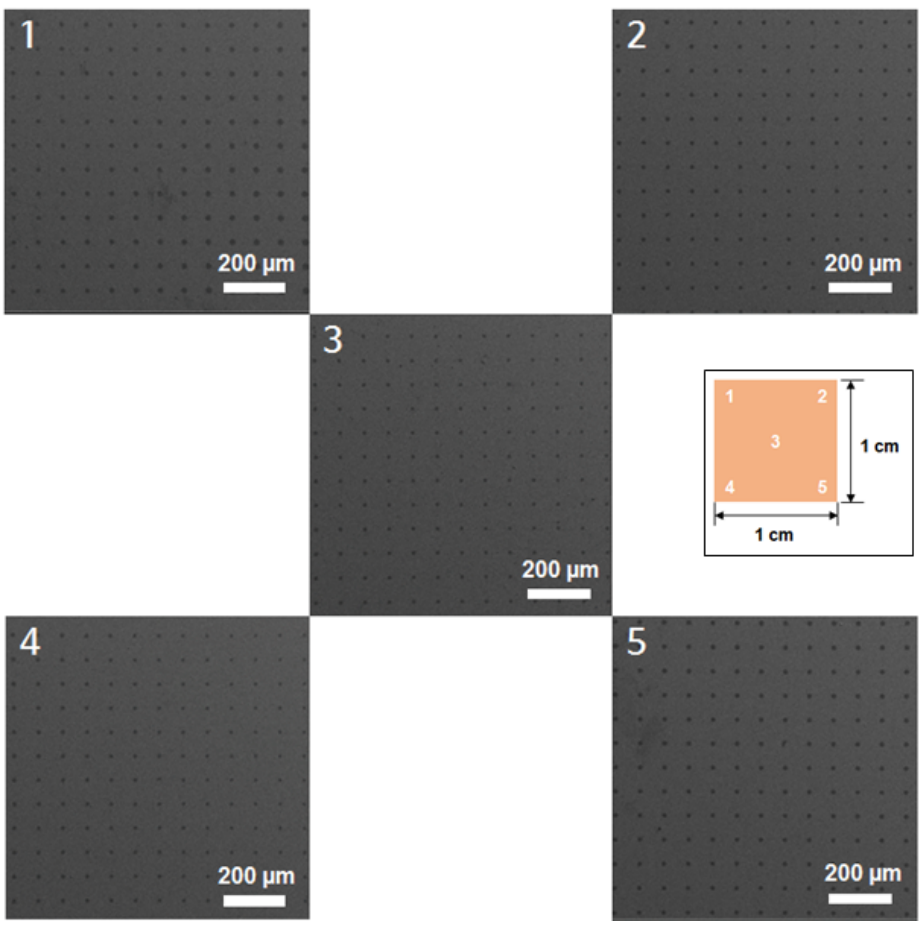

Figure 4.12. SEM images for large area assembly of charged nanoparticle via electrified mask. The numbers of images indicate a position at the substrate as illustrates in right small box

The charged nanoparticles from the multi-spark discharger were injected into deposition chamber uniformly in the large area. Then, the charged nanoparticles were dragged to the electrified mask by electric attraction. The charged nanoparticles guided into the substrate with smaller width than mask opening through the large area electrostatic lenses which were generated from large area polymer electrified mask.

When the charged nanoparticles assembled by the electrified mask, the focusing ratio can be controlled by adjusting potential difference between the electrode and the electrified mask (Choi et al. 2015). Figure 4.13 shows electric field simulation results depends on the potential difference between the electrode and the electrified mask. When the potential difference is zero, all electric stream lines are converged into the electrified mask since it could not generate spatial difference of electric potential (Figure 4.13a). The stream lines of electric field thinly converged as increase of potential difference between the electrode and the electrified mask (Figure 4.13b-d).

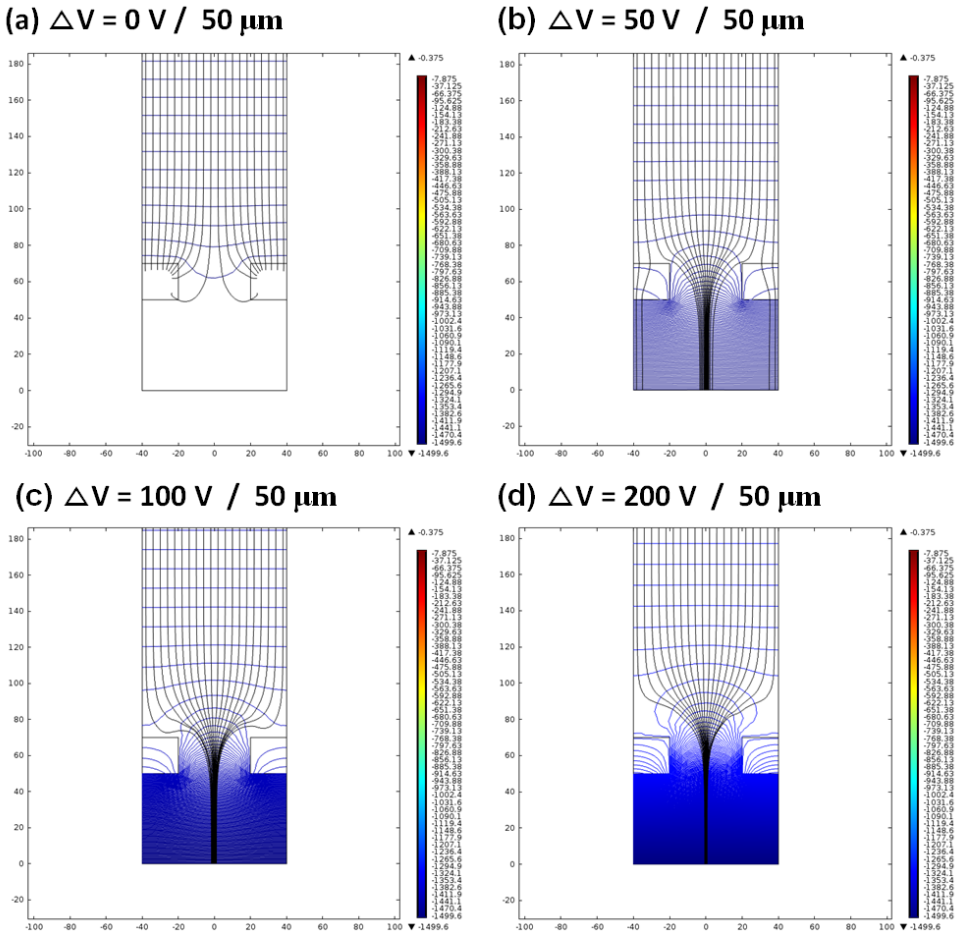

Figure 4.13. Electric field simulation results depend on electric potential difference between the electrode and the electrified mask

Figure 4.14 shows experimental results for control of focusing ratio by adjusting potential difference between the electrode and the electrified mask. In the case of zero potential difference, all nanoparticles were not deposited on a substrate. This is a same result as the electric field simulation. The focusing ratio was varied from 1.11 to 3.33 as increase of potential difference between the electrode and the electrified mask. From these results, we can show that control of focusing ratio is possible through large area polymer electrified mask.

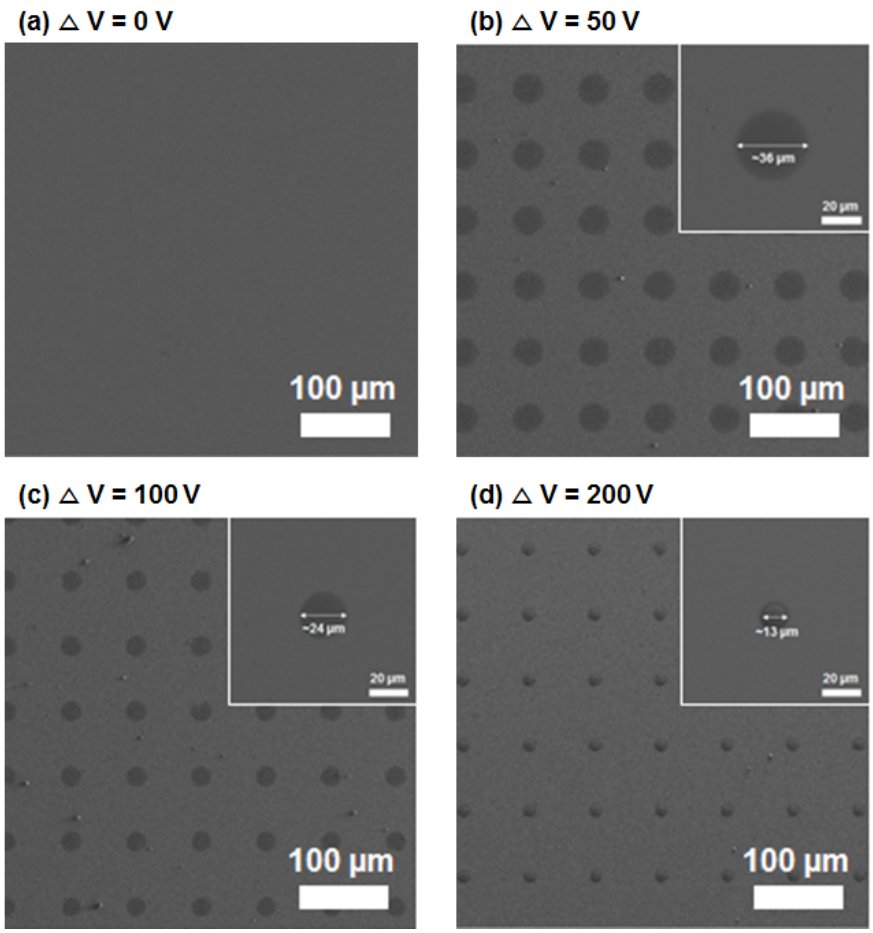

Figure 4.14. Variation of focusing ratio depends on the potential difference between the electrode and the electrified mask

4.4.2. Electric field calculation for the determination of electric potential values at the electrified mask in the case of a non-conducting substrate

For generation of the electrostatic lens, spatial difference of electric potential is needed. In the case of a conducting substrate, the potential difference between the substrate and the mask surface is easily determined by direct application of electric potential at the substrate ($V_{substrate}$) and the electrified mask (V_{mask}) because the $V_{substrate}$ is same as the $V_{electrode}$ (Figure 4.15a). However, in the case of a non-conducting substrate, the electric potential on the substrate cannot be applied directly because the $V_{substrate}$ is not equal to the $V_{electrode}$. Therefore, electric field simulation should be conducted to determinate mask potential values for desired potential difference (Figure 4.15b).

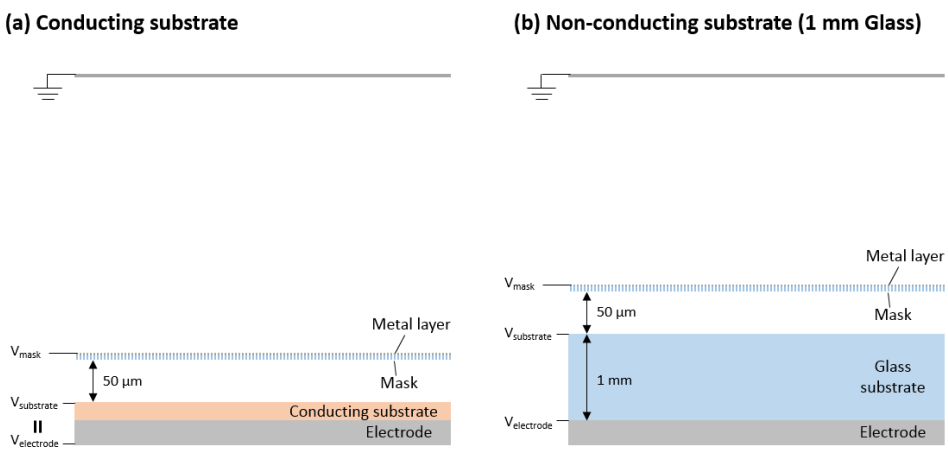

Figure 4.15. Determination of the electric potential value at the electrified mask. (a) conducitng substrate case and (b) non-conducting substrate case

The electric field simulation results for a non-conducting substrate case are shown at Figure 4.16. The large elecric potential difference between the $V_{electrode}$ and the V_{mask} is needed for desired potential difference between the $V_{substrate}$ and the V_{mask} due to prescence of thick non-conducting substrate. Figure 4.16a shows electric field results when the $V_{electorde}$ is -1500 V which is same value as that of conducting substrate case. Since the V_{mask} is limited below the ground (V=0), the electric potential difference between the V_{mask} and the $V_{substrate}$ is also limited. Therefore, in the case of non-conducting substrate, higher applied potential of the electrode is needed to expand control range of electrod static lens. Figure 4.16b shows electric field results when electrode potential is -4000 V. When -2400 V of mask potential is applied, the difference between the V_{mask} and the $V_{electrode}$ is about 300 V in 50 μm distance.

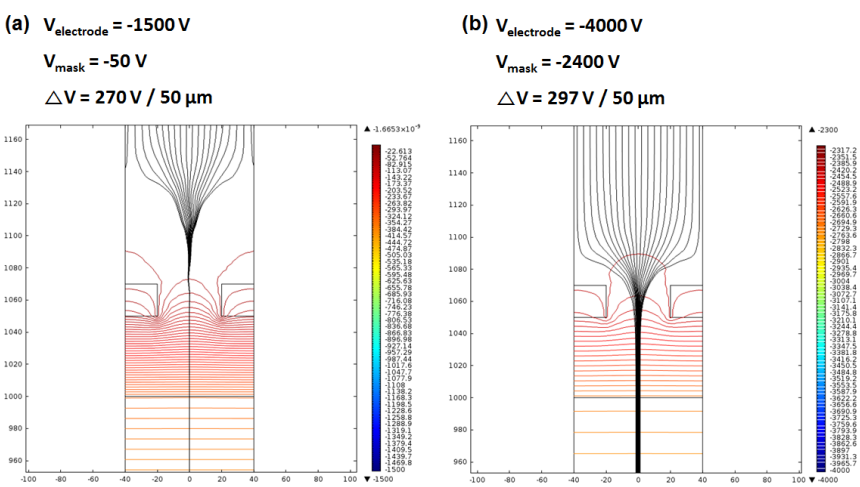

Figure 4.16. Electrostatic lens formation on a non-conducting substrate via electrified mask when the electric potential of electrode is (a) -1500 V and (b) -4000 V

4.4.3. Charged nanoparticle assembly on a non-conducting substrate by eliminating ions via electrified mask

In the previous Chapters, we found out that the ion accumulation is a key parameter of charged nanoparticle assembly on a non-conducting substrate. When the charged nanoparticle was assembled through electrified mask, the ion accumulation affected to electric field formation in different way from previous ion-assisted aerosol lithography method. Figure 4.17 shows electric field formation as increase of surface charge density in previous ion-assisted aerosol lithography method. Figure 4.17a and b present insufficient ion accumulation to generate electrostatic lens. When enough ions are accumulated, electrostatic lens is well generated even though the charges on a non-conducting substrate could not escape as explained at Chapter 3 (Figure 4.17c). Even in the case of excessive accumulation of ions on a non-conducting substrate (Figure 4.17d), there is no problem to generate electrostatic lens.

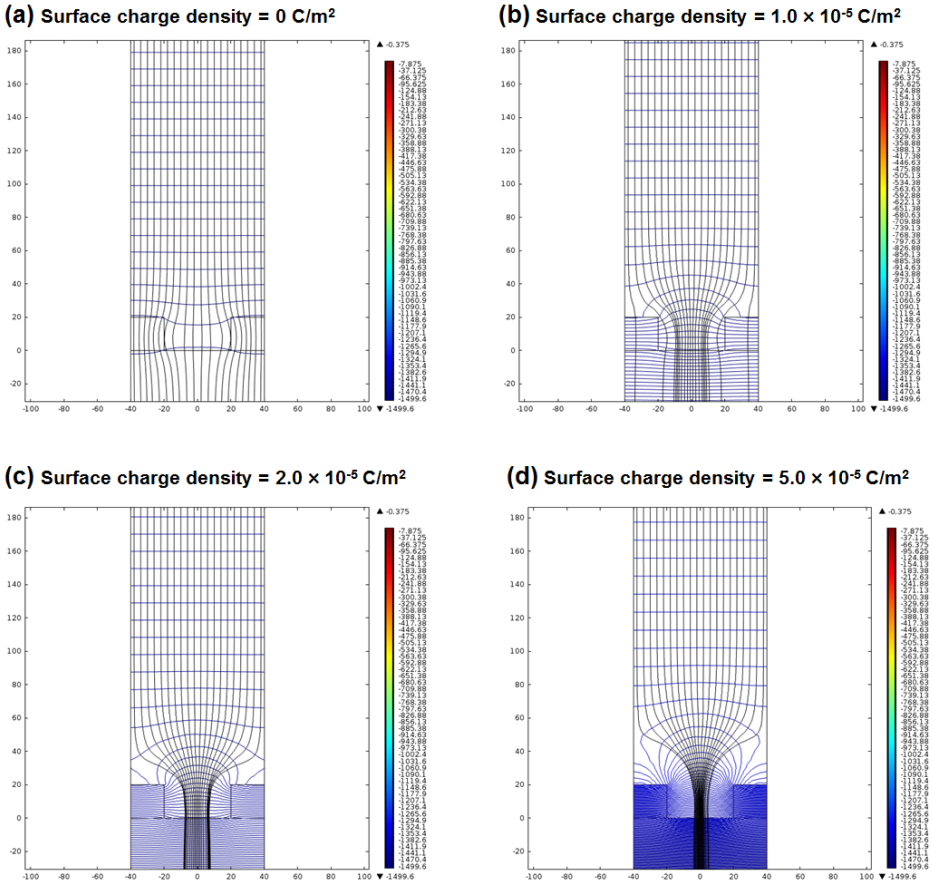

Figure 4.17. Electric field formation as increase of surface charge density in the previous ion-assisted aerosol lithography method

In initial stage of the previous ion-assisted aerosol lithography method, accumulated ions only affect to electric potential value on a substrate. Figure 4.18 shows variation of electric field strength depends on the surface charge density on a non-conducting substrate. The electric field strength was obtained from electric potential results along the y-axis of the electric field simulation. As increase of surface charge density on a non-conducting substrate, the electric potential values on a non-conducting substrate is increased. As a result, electric field strength is decreased from 74949.18 V/m to 70638.14 V/m as increase of surface charge density from 0 C/m^2 to 5.0×10^{-5} C/m^2. It means that higher voltage should be applied to the electrode for attraction of nanoparticles when the ion-assisted aerosol lithography was conducted on a non-conducting substrate.

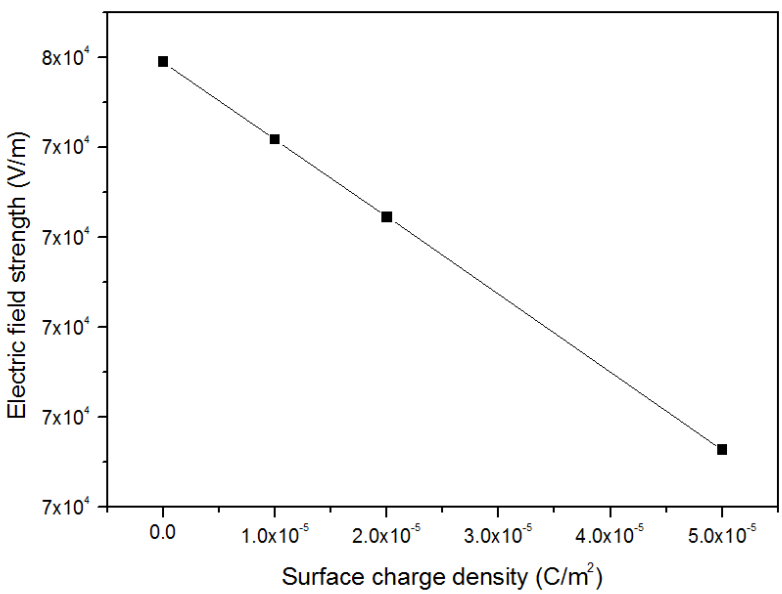

Figure 4.18. 1-D plot of electric potential values along the y-axis in electric field simulation of previous ion-assisted aerosol lithography method

Figure 4.19 present electric field simulation results of electrified mask method depending on surface charge density on a non-conducting substrate. Since electrified mask method do not need ions for generation of electrostatic lens, electrostatic lens is well generated without ion accumulation as shown at Figure 4.19a. However, electric field is getting distorted as increase of surface charge density on a non-conducting substrate. Consequently, all of the electric field streamlines cannot reach to a non-conducting substrate (Figure 4.19d). Unlike previous ion-assisted aerosol lithography method, fixed electric potential exist at a surface of electrified mask. When the surface charge density on a non-conducting substrate is zero, the fixed electric potential generated the electrostatic lens. However, the increase of surface charge density on a non-conducting substrate cause enhancement of electric potential on a non-conducting substrate. Thus, the increased electric potential on a non-conducting substrate let the fixed electric potential attract the incoming nanoparticles, because the direction of the electric force is toward lower electric potential. Electric potential values at the height of mask surface are plotted at Figure 4.20. As the surface charge is increased, the electric potential at the mask opening is also increased. Consequently, when the surface charge density is 6.0×10^{-5} C/m^2, the electric potential at the mask opening become larger than the fixed mask potential, and it makes incoming particles attract to the mask.

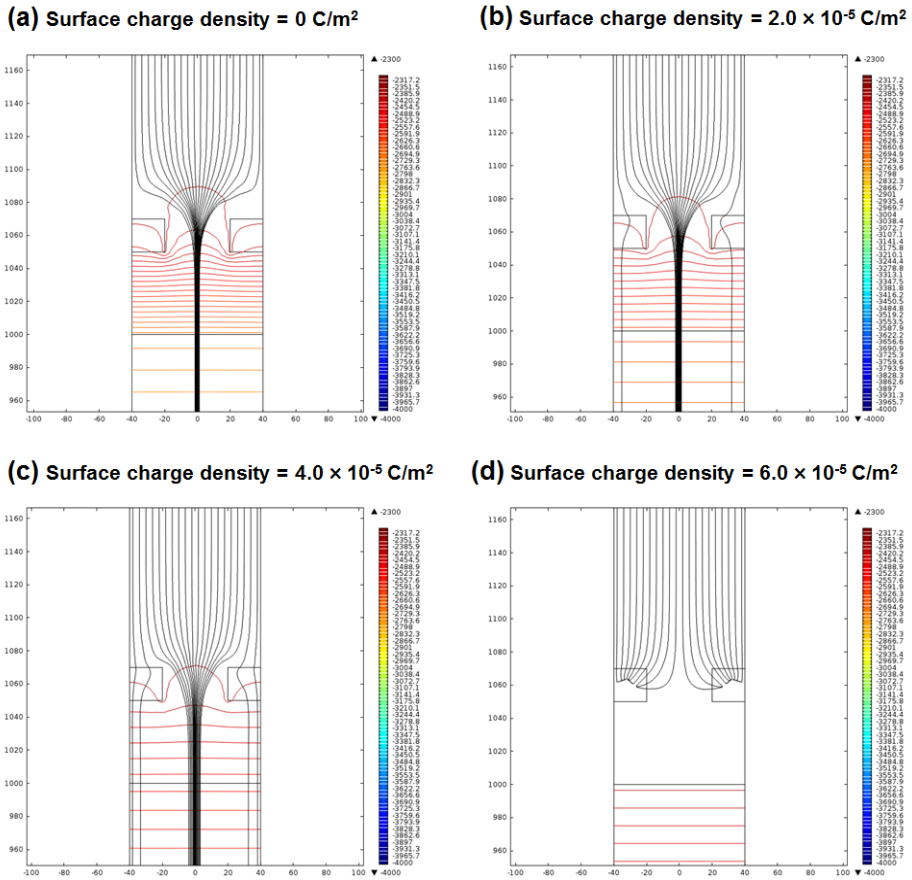

Figure 4.19. Electric field formation as increase of surface charge density in the electrified mask method

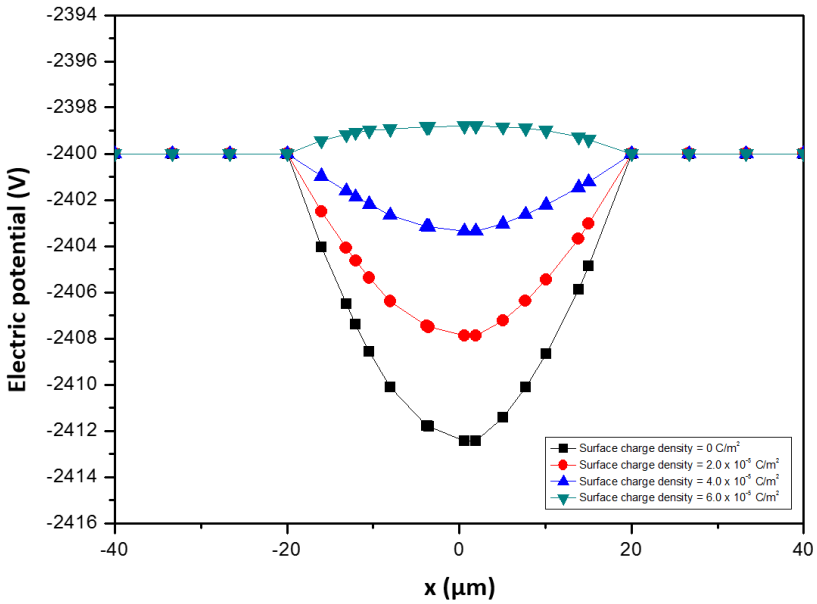

Figure 4.20. 1-D plot of electric potential at the height of mask surface depends on surface charge density on a non-conducting substrate

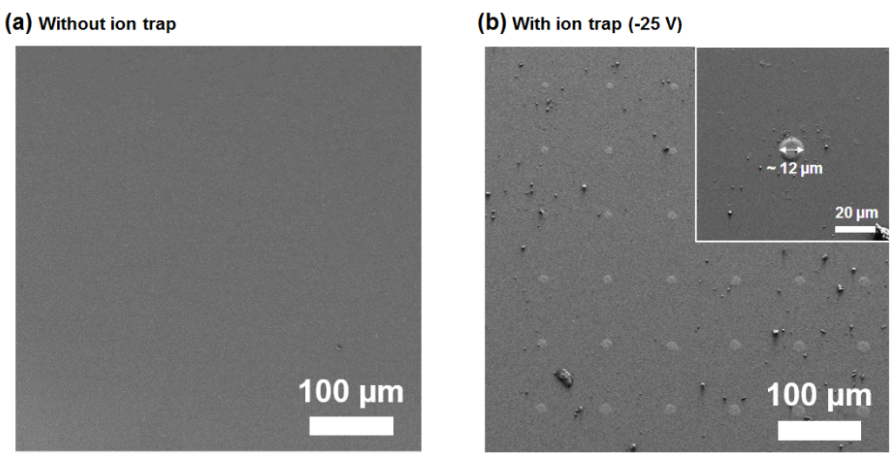

Figure 4.21. Experimental results of charged nanoparticle assembly on a non-conducting substrate when (a) the ion trap turned off and (b) ions were eliminated by ion trap with -25 V.

Figure 4.21 shows experimental result of charged nanoparticle assembly on a non-conducting substrate. When the ion trap turned off, there was no particles on a non-conducting substrate because all of the particles were attracted to the electrified mask as shown at electric field simulation results (Figure 4.21a). Thus, ion accumulation should be prevented to assembly of charged nanoparticles on a non-conducting substrate via electrified mask. Figure 4.21b shows SEM results of charged nanoparticle assembly on a non-conducting substrate when the nitrogen ions were eliminated by ion trap. 99.902% of ions were captured by ion trap with -25 V of ion trap voltage (Figure 3.9). Because the electrified mask do not required ions for electrostatic lens generation, charged nanoparticles were well focused into the mask opening. The focusing ratio at that condition is about 3.33.

Next, we have to show that the focusing ratio is also controlled on a non-conducting substrate because the biggest benefit of electrified mask is precise control of focusing ratio. The various potential values at the mask was determined by electric field simulation (Figure 4.22a-c). The applied potentials to the mask (V_{mask}) of each cases are determined as -3450 V, -2900 V, and -2400 V, in order to make the potential difference between the mask and the substrate of each cases are about 103 V, 204 V, and 297 V. The electric field simulation results shows that the electric field streamline are more focused by increasing of the potential difference. The experimental results of each cases are shown at Figure 4.23d-f. As the potential difference increased, the smaller size of particle assembly are observed. The focusing ratio of each cases are 0.8, 1.42, and 3.33, respectively. Although it shows slightly different results from the conducting substrate cases with similar potential difference, it is reasonable results by considering the error range of simulation. In the case of Figure 4.23d, the size of assembled pattern was larger than the size of mask opening. The charged particles are diffused after enter the mask opening by Brownian random

motion. Consequently, we can demonstrate that the charged particle assembly on a non-conducting substrate can be achieved via electrified mask with elimination of ions. In addition, the focusing ratio is also controlled by manipulating applied potential of the mask even in the case of a non-conducting substrate.

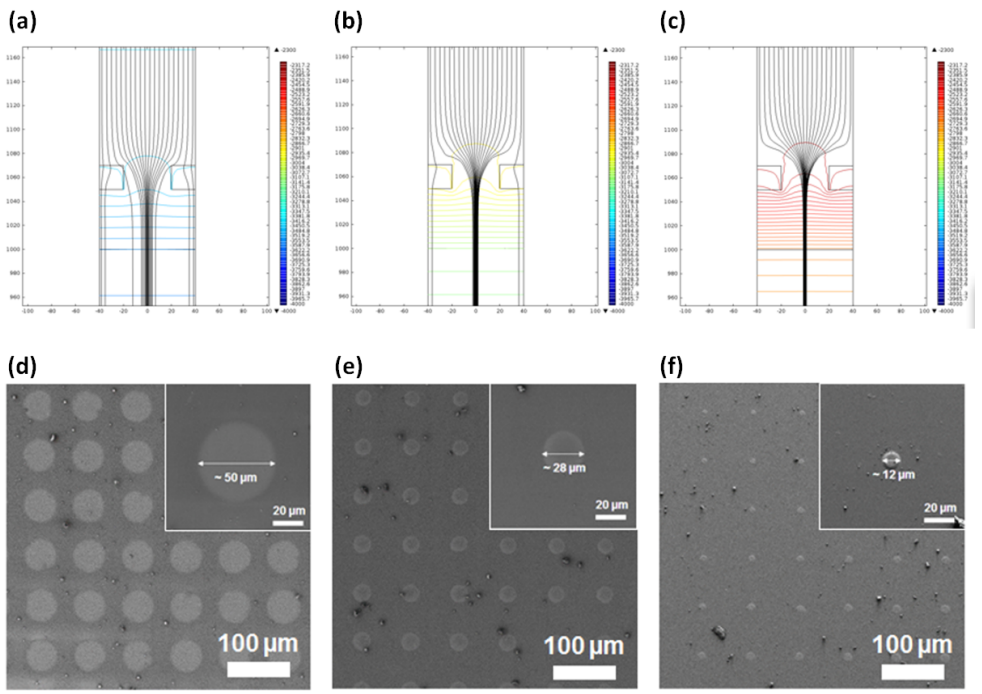

Figure 4.22. Electric field simulation and experimental results for control of focusing ratio on a non-conducting substrate. The potential difference between the mask and the substrate are about (a), (d) 103 V, (b), (e) 204 V and (c), (f) 297 V, respectively

4.4.4. Characteristics of the electrostatic lens formation via electrified mask

As mentioned above, formation of the electrostatic lens are originated from spatial electric potential difference. In the electrified mask method, the spatial electric potential difference can be manipulated by applying electric potential values at the electrified mask surface. In order to generalize characteristics of electrostatic lens formation in various experimental conditions for instance substrate types, electrode voltages and etc., we should consider the main parameter which determines the characteristics of it.

In order to understand principle of electrostatic lens formation, we calculated electric field with/without the electrified mask (Figure 4.23). The electric potential values were plotted along the y-axis at the position of the opening and the mask (Figure 4.23a). Figure 4.23b shows electric potential values along the y-axis with/without the electrified mask at the position of the mask. When the electrified mask was not exist, the electric potential values were reduced constantly from $V_{substrate}$ to the ground (V=0). Thus, the uniform electric field strength was generated along the y-axis. However, when the electrified mask was existed with fixed V_{mask}, the electric field strength along the y-axis were shown two different values by the V_{mask}. Strong electric field was generated under the mask, while weak electric field was generated over the mask by the fixed V_{mask}. Figure 4.23c shows electric potential values along the y-axis at the position of the opening and the mask with electrified mask. The result shows that the strong electric field strength from the fixed V_{mask} caused electric potential difference along the x-axis. As a result, the x-directional electric force was applied to the charged nanoparticles by the electric potential difference. Consequently, the difference of electric field strength between the over

and the under mask generated the electrostatic lens by inducing electric potential differences along the x-direction.

Therefore, we supposed that the main parameter which determines characteristics of the electrostatic lens formation is a ratio of the electric field strength between the over and the under mask, and the ratio of electric field strength was defined as

$$r_e = \frac{E_{um}}{E_{om}} \tag{4.2}$$

where, E_{um} is the electric field strength under the mask ($E_{um} = V_{mask}/H$) and E_{om} is the electric field strength over the mask ($E_{om} = (V_{substrate} - V_{mask})/h$).

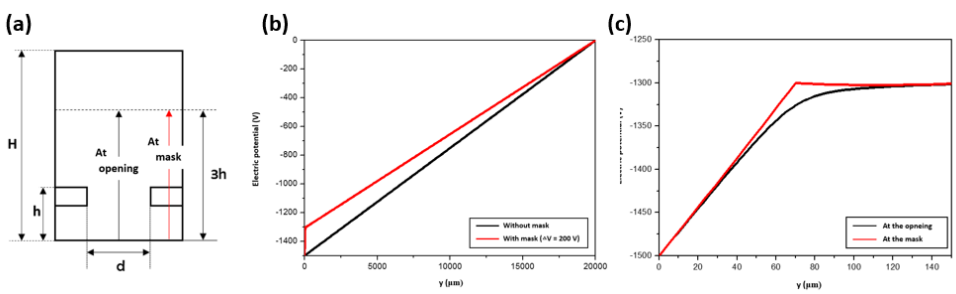

Figure 4.23. (a) Geometry of electric field simulation area. (b) Electric potential values along the y-axis with/without the electrified mask at the position of mask opening. (c) Electric potential values along the y-axis (y=0 to 3h) in the case at the opening and the mask

Figure 4.24 shows electric field simulation results in different experimental conditions (electrode voltage) with same r_e. Although the experimental condition was different, exactly same electric fields were generated with same r_e. Hence, we can verify that the characteristics of electrostatic lens formation via electrified mask method was represented by the r_e.

(a) $V_{electrode}$ = -1500 V

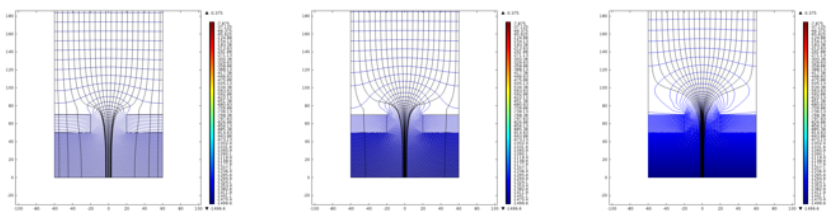

ΔV	50 V	100 V	200 V
r_e	13.7586	28.5002	61.3845

(b) $V_{electrode}$ = -750 V

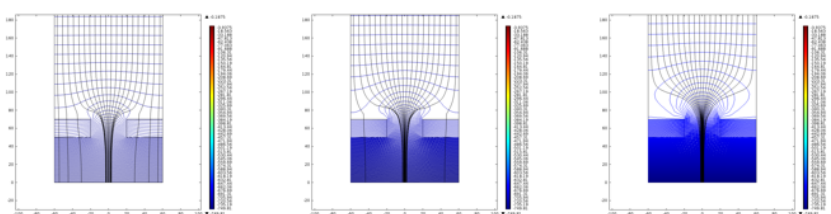

ΔV	25 V	50 V	100 V
r_e	13.7586	28.5002	61.3845

Figure 4.24. Electric field simulation results in different experimental conditions with same r_e. (a) $V_{electrode}$ = -1500 V and (b) $V_{electrode}$ = -750 V

4.5. Conclusion

In this work, we designed large area charged particle assembly system including ion elimination instruments for the applicability expansion of electrified mask to a non-conducting substrate. The large area charged particle assembly systems were comprised with multi-spark dischargers for the large area spray of charged nanoparticles and polymer electrified mask for the large area generation of electrostatic lenses. For the particle deposition on a non-conducting substrate, all of the nitrogen ions which are by-product of charged nanoparticle were completely eliminated by ion trap with -25 V of ion trap voltage. The electric potential value at the mask surface was determined through electric field simulation. Consequently, the charged particle assembly on a non-conducting substrate was obtained via large area electrified mask system with the ion elimination. Moreover, we demonstrated that the focusing ratio could be controlled by manipulating applied potential of the mask even in the case of a non-conducting substrate. Therefore, we successfully developed electrified mask system into a large area and a non-conducting substrate system.

Chapter 5.

Concluding Remarks

Ion-assisted aerosol lithography has been developed a lot since it was first reported. At first, two-dimensional nanoparticle arrays could be obtained with much smaller size of assembly than that of pre-pattern opening. After that, three-dimensional nanoparticle structures could be produced through continuous deposition of nanoparticles by using antenna effects. Moreover, high-resolution arrays were achieved by sequential operation of ion-induced focusing mask, and the electrified mask enable precise control of focusing ratio. In this study, we recognized necessity of understanding about ion-assisted aerosol lithography on a non-conducting substrate for the wide use of this method. Hence, we have investigated the research about ion-assisted aerosol lithography on a non-conducting substrate for in-depth understanding of it.

When the nanoparticles were assembled on a non-conducting substrate via previous ion-assisted aerosol lithography method, the growth of nanoparticle structures were terminated with repulsion of incoming particles from the nanoparticle structures. Through electric field simulation, we demonstrated that charge accumulation on nanoparticle structures caused electric field distortion which ultimately brought termination of nanoparticle structure growth.

In order to control accumulated charges on nanoparticle structures, we designed ion trap for manipulation of ion inflow. The ions were selectively captured by electrical mobility difference between ions and nanoparticles. Through optimization of ion inflow, the continuous growth of three-dimensional nanoparticle structures could have been obtained. The effect of charge accumulation on nanoparticle structures and resist surface was elucidated by electric field simulation. Consequently, by controlling ion accumulation, we successfully fabricated three-dimensional nanoparticle structures on a non-conducting substrate via ion-assisted aerosol lithography.

Based on the understanding of ion-assisted aerosol lithography on a non-conducting substrate, we conducted a study about electrified mask method on a non-conducting substrate. In addition, large area electrified mask method system was also suggested for practical use of this method. At first, multi-spark discharger and large area polymer electrified mask were used to achieve the large area electrified mask method system. Second, all the ions were eliminated by ion trap for application of electrified mask method to a non-conducting substrate because electrified mask does not require ion accumulation for generation of electrostatic lenses. Consequently, we showed that electrified mask method is applicable to a non-conducting substrate. Moreover, precise control of focusing ratio was also achieved on a non-conducting substrate.

References

1. Burm KTAL (2007). Calculation of the Townsend Discharge Coefficients and the Paschen Curve Coefficients. Contributions to Plasma Physics 47:177-182.
2. Chae S, Lee D, Kim MC, Kim DS, Choi M A study of a Wire-in-hole Type Spark Discharge Generator for Consistent Generation of Unagglomerated Nanoparticles. In: 2014 International Aerosol Conference, BEXCO, Busan, Korea, 2014.
3. Cheng DK (1989). Field and Wave Electromagnetics 2nd edition. Addison-Wesley, New York.
4. Choi H, Kang S, Jung W, Jung Y-h, Park SJ, Kim DS, Choi M (2015). Controlled electrostatic focusing of charged aerosol nanoparticles via an electrified mask. Journal of Aerosol Science 88:90-97.
5. Demirors AF, Pillai PP, Kowalczyk B, Grzybowski BA (2013). Colloidal assembly directed by virtual magnetic moulds. Nature 503:99-103.
6. Ergin T, Stenger N, Brenner P, Pendry JB, Wegener M (2010). Three-Dimensional Invisibility Cloak at Optical Wavelengths. Science 328:337-339.
7. Guo CX, Wang M, Chen T, Lou XW, Li CM (2011). A Hierarchically Nanostructured Composite of MnO2/Conjugated Polymer/Graphene for High-Performance Lithium Ion Batteries. Adv Energy Mater 1:736-741.
8. Han K, Kim W, Yu J, Lee J, Lee H, Woo CG, Choi M (2012). A study of pin-to-plate type spark discharge generator for producing unagglomerated nanoaerosols. Journal of Aerosol Science 52:80-88.

9. Hinds WC (1999). Aerosol technology: Properties, behavior and measurement of airborne particles. Wiley, New York.
10. Jiang L, Wang W, Fuchs H, Chi L (2009). One-Dimensional Arrangement of Gold Nanoparticles with Tunable Interparticle Distance. Small 5:2819-2822.
11. Kalsin AM, Fialkowski M, Paszewski M, Smoukov SK, Bishop KJM, Grzybowski BA (2006). Electrostatic Self-Assembly of Binary Nanoparticle Crystals with a Diamond-Like Lattice. Science 312:420-424.
12. Kim D, Pikhitsa PV, Yang H, Choi M (2011). Room temperature CO and H 2 sensing with carbon nanoparticles. Nanotechnology 22:485501.
13. Kim H, Kim J, Yang H, Suh J, Kim T, Han B, Kim S, Kim DS, Pikhitsa PV, Choi M (2006). Parallel patterning of nanoparticles via electrodynamic focusing of charged aerosols. Nat Nanotechnol 1:117-121.
14. Kraus T, Malaquin L, Schmid H, Riess W, Spencer ND, Wolf H (2007). Nanoparticle printing with single-particle resolution. Nat Nanotechnol 2:570-576.
15. Lee H, You S, Pikhitsa PV, Kim J, Kwon S, Woo CG, Choi M (2011). Three-Dimensional Assembly of Nanoparticles from Charged Aerosols. Nano Lett 11:119-124.
16. Lee H, You S, Woo CG, Lim K, Jun K, Choi M (2009). Focused patterning of nanoparticles by controlling electric field induced particle motion. Applied Physics Letter 94.
17. Li A, Ahmadi G (1992). Dispersion and Deposition of Spherical Particles from

Point Sources in a Turbulent Channel Flow. Aerosol Science and Technology 16:209-226.

18. Lin Y, Skaff H, Emrick T, Dinsmore AD, Russell TP (2003). Nanoparticle Assembly and Transport at Liquid-Liquid Interfaces. Science 299:226-229.
19. Nykypanchuk D, Maye MM, van der Lelie D, Gang O (2008). DNA-guided crystallization of colloidal nanoparticles. Nature 451:549-552.
20. Park M-H, Kim K, Kim J, Cho J (2010). Flexible Dimensional Control of High-Capacity Li-Ion-Battery Anodes: From 0D Hollow to 3D Porous Germanium Nanoparticle Assemblies. Adv Mater 22:415-418.
21. Ponzoni A, Comini E, Sberveglieri G, Zhou J, Deng SZ, Xu NS, Ding Y, Wang ZL (2006). Ultrasensitive and highly selective gas sensors using three-dimensional tungsten oxide nanowire networks. Appl Phys Lett 88.
22. Su B, Zhang C, Chen S, Zhang X, Chen L, Wu Y, Nie Y, Kan X, Song Y, Jiang L (2014). A General Strategy for Assembling Nanoparticles in One Dimension. Adv Mater 26:2501-2507.
23. Visser J (1972). On Hamaker constants: A comparison between Hamaker constants and Lifshitz-van der Waals constants. Advances in Colloid and Interface Science 3:331-363.
24. von Freymann G, Ledermann A, Thiel M, Staude I, Essig S, Busch K, Wegener M (2010). Three-Dimensional Nanostructures for Photonics. Adv Funct Mater 20:1038-1052.
25. Vyawahare S, Craig KM, Scherer A (2006). Patterning Lines by Capillary Flows.

Nano Lett 6:271-276.

26. Wolf H, Birringer R (2005). Pattern formation in an array of magnetic nanoscale rods mimics magnetic-dipole interaction-driven spinodal decomposition. J Appl Phys 98.

27. You S, Han K, Kim H, Lee H, Woo CG, Jeong C, Nam W, Choi M (2010). High-Resolution, Parallel Patterning of Nanoparticles via an Ion-Induced Focusing Mask. Small 6:2146-2152.

28. Zhang Y, Grady NK, Ayala-Orozco C, Halas NJ (2011). Three-Dimensional Nanostructures as Highly Efficient Generators of Second Harmonic Light. Nano Lett 11:5519-5523.

Abstract (in Korea)

비전도성 기판에서의 하전된 나노 입자의 조립

서울대학교 대학원 기계항공공학부

강승현

나노 입자 조립 기술은 building block 인 나노 입자의 직접적인 제어를 통해 구조물을 형성하는 기술로, 이렇게 만들어진 구조물의 독특한 성질로 인해 과학, 공학분야에서 많은 관심을 받으며 연구가 진행되고 있다. Ion-assisted aerosol lithography 는 에어로졸 기반의 다목적의 유용한 나노 입자 조립 기술이다. 이러한 ion-assisted aerosol lithography 기술은 그 동안 많은 발전이 있었음에도 불구하고 비전도성 기판에서의 이 기술에 대한 연구는 아직 충분히 이루어지지 않았다. 본 연구에서는 ion-assisted aerosol lithography 방법의 적용 가능성을 확대하기 위해서는 비전도성 기판에서의 이 기술에 대한 심도 있는 이해가 필요함을 느끼고, 이에 대한 연구를 수행하였다.

가장 먼저, 비전도성 기판에서의 나타나는 ion-assisted aerosol lithography 기술의 특성을 파악하기 위한 연구를 수행하였고, 그 결과 비전도성 기판에서는 나노 입자 구조물이 성장과정 중에 성장을 멈추고 후속 입자들이 구조물로부터 밀려나는 현상을 발견할 수 있었다. 전기장 계산을 통하여 이러한 실험 결과를 뒷받침 하였고, 구조물에 축적된 전하에 의해 전기장이 변형되어 추가적인 입자의 증착을 막는 다는 것을 확인 할 수 있었다.

이러한 나노 입자 구조물의 전하 축적을 제어하기 위하여, 이온 트랩을

설계하였다. 이 이온트랩을 이용한 이온 유입량 최적화를 통해, 구조물의 계속된 성장을 유도할 수 있었다. 이러한 이온 유입량 최적화 결과는 나노 입자 구조물과 레지스트 표면의 전하축적에 의한 힘의 균형으로 설명할 수 있었으며, 전기장 시뮬레이션을 통해 이를 확인할 수 있었다.

비전도성 기판에서의 ion-assisted aerosol lithography 기술의 이해를 바탕으로, electrified mask 방법을 대면적의 비전도성 기판에 적용 가능하도록 발전 시켰다. 멀티-스파크 방전기와 대면적의 polymer electrified mask 를 이용하여 대면적의 하전된 입자 조립 시스템을 구성하였다. Electrified mask 방법은 정전기적 렌즈 형성에 이온 축적이 필요하지 않기 때문에, 이를 비전도성 기판에 적용하기 위해서 이온트랩을 이용하여 모든 이온을 제거하였다. Electrified mask 에 가해주는 전압 값은 전기장 시뮬레이션을 계산을 통하여 얻을 수 있었다. 결론적으로, 이 방법을 통하여 비전도성 기판에서도 electrified mask 를 이용한 하전 된 입자 조립이 가능함을 보일 수 있었고, electrified mask 에 가해준 전압 값을 제어함으로써 비전도성 기판에서도 집속 정도를 정밀하게 제어할 수 있음을 보였다.

주요어: 나노입자 조립, 비전도성 기판, ion-assisted aerosol lithography, 이온 트랩, electrified mask

학번: 2009-20649